Deliverable 4.5
Modelled flow fields, turbulence and residence time in experimental units

Version 1

WP 4
Deliverable 4.5
Lead Beneficiary: NTNU
Call identifier: Biological and Medical Sciences - Advanced Communities: Research infrastructures in aquaculture
Topic: INFRAIA-01-2018-2019
Grant Agreement No: 871108
Dissemination level: PU
Date: 30.09.2024

This project has received funding from the European Union's Horizon 2020 research and innovation programme under grant agreement No. 871108 (AQUAEXCEL3.0). This output reflects only the author's view and the European Commission cannot be held responsible for any use that may be made of the information contained therein.

Contents

1. Objective

The purpose of this document is to describe the flow field model in terms of flow fields, turbulence and calculated residence times. This model is one of the main components in the AQUAEXCEL3.0 virtual laboratory developed in Task 4.1 - *Virtual Laboratories and modelling tools for designing experiments in aquaculture research facilities.*

The main components of the virtual laboratory are:

- Growth, nutrition and waste production models for different fish species
- Water quality and water treatment model
- Model of hydrodynamic flow fields in tanks and cages
- Fish behaviour

The objective of the flow field model is to represent the water currents within the production unit - fish cage or tank, presenting key information relating to the current to the other model components.

2. Background

This report is part of AQUAEXCEL3.0 WP4/Joint Research Activity 1 - *Technological tools for improved experimental procedures*. Task 4.1 - *Virtual Laboratories and modelling tools for designing experiments in aquaculture research facilities* aims to extend the Virtual Laboratory developed in AQUAEXCEL2020 as a general tool for designing and simulating virtual complex experiments in advance of a trial by: 1) adding a new model of fish behaviour, 2) expanding the growth model and applying it to new species, 3) improving the flow model, 4) expanding the water quality model to include CO2 and pond systems, and 5) enhancing the user experience by improving decision support through an Artificial Agent.

The focus of Subtask 4.1.3 has been to provide Computational Fluid Dynamics (CFD) simulations of the hydrodynamic conditions in selected experimental units, making a validation study of stationary CFD modelled flow against experimental data, and using the model to calculate Residence Time Distribution for dissolved material and solid particles (representing feed pellets and faeces) to extract information related to the self-cleaning capacity of experimental tanks.

The Virtual Laboratory also supports simulations of experiments in open sea cages. The flow field model provides representative vertical current speed profiles with optional tidal variability in this case. Flow fields in sea cages have not been a focus area in the AQUAEXCEL3 project, but for completeness we provide in this report a description of the model as developed in the AQUAEXCEL2020 project.

3. Methodology

3.1. Survey of tank designs

In order to get an overview of the typical range of experimental units for aquaculture research, a survey of AQUAEXCEL3 partners was conducted. The survey aimed to gather key information about the experimental units in each research facility. It was distributed to all AQUAEXCEL3 partners in the form of an Excel sheet.

The information to request was determined based on a discussion between NTNU, JU and Nofima based on what information would be useful for the decision of which tank designs to model, and for the process of setting up the CFD model. For each tank design, the following information was requested:

- **Basic information:** name of facility, species, FT/RAS, tank type and shape, number of tanks
- **Tank dimensions:** volume (L), height (cm), waterline height (cm), width (cm), diameter (cm), bottom angle (degrees)
- **Water inlets:** position, dimension (mm diameter), design of inlet column (nozzles, holes or single opening face), directional angle of inlet column
- **Water outlets:** position, dimension (mm diameter)
- **Flow:** maximum water exchange rate (L/h), internal parameters affecting flow conditions (e.g. centre pipes), available experimental data for flow conditions (yes/no)
- **Other:** picture available, additional comments/explanations

The distribution of the survey and gathering of results was conducted under Subtask 4.1.6. Responses were received from 7 partners (HCMR, University of Stirling, IEO, INRAE, UNITO, CSIC and IFREMER), and a total of 107 unit types were described. These included units for fish, octopus, shellfish, and plankton. 41 were listed as round, cylindrical or circular, 33 as rectangular or square, 4 as cylindroconical and 5 as raceways or similar. The tank designs were distributed over a wide range of sizes (Figure 1).

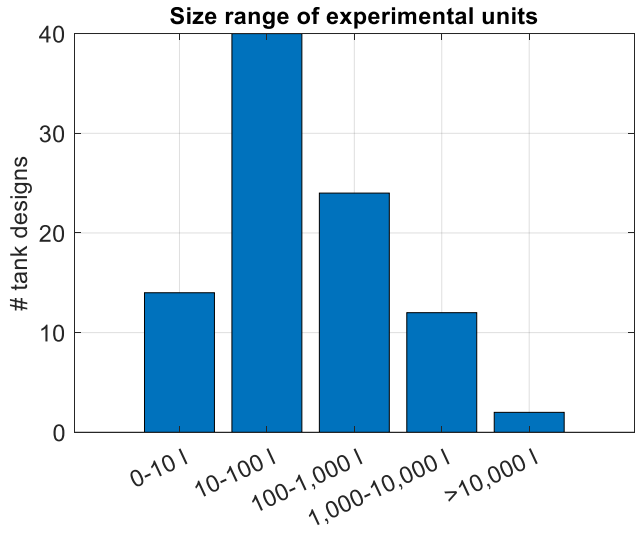

Figure 1: Distribution of reported tank sizes

3.2. Flow fields in tanks

Flow fields in aquaculture tanks has received significant attention in the research community, as the flow is crucial to achieve sufficient water exchange, supply of oxygen and flushing of nitrogenous waste, cleaning of uneaten feed pellets and faeces from the fish, in addition to providing flow conditions suitable for the swimming pattern and swimming capacity of the fish. Flow fields depend on water exchange rate, tank size and shape, as well as the inlet and outlet structures, as reviewed for circular tanks by Timmons et al. (1998).

3.2.1. Flow field modelling

Computational Fluid Dynamics (CFD) models can be used to compute flow fields in tanks disregarding the effect of the fish (Sayma, 2009). The fundamental basis of CFD models is the Navier-Stokes equations which describe the motion of viscous fluids. CFD models solve a form of Navier-Stokes numerically after discretizing the simulation volume, typically using non-uniform discretization schemes where the spatial resolution varies over the simulated volume with higher resolution around features that cause strong local variations in the flow field, such as inlets. The process of designing the model grid is a separate operation from the CFD simulation itself, and this operation may require significant computational power. Numerical solution of the equations on the model grid is also computationally highly demanding, and models are typically parallelized and run on high performance computing centres. The output (computed 3D flow field and related hydrodynamic quantities) may be either steady state (independent of time) or dynamic (time-dependent). For flow fields in tanks, we

are looking for the steady-state field for a given tank setup and water in-flow rate, so the CFD model will be run to produce a constant 3D field representing steady state flow. The field may be accompanied by a computed turbulence kinetic energy field describing the level of turbulence estimated over the volume.

There is a wide selection of open source software (e.g. OpenFoam, Typhon and Reef3D) and commercial software (e.g. Ansys Fluent, CFX and COMSOL) that basically solve the same mathematical equations but have different features and different learning curves.

Based on the comparison of experimentally measured and simulated values of velocity profiles, we argue that the CFD code ANSYS Fluent represents a modern and reliable tool for the simulation of hydrodynamic flow field within a production unit, although it does not have the option of simulating the effect of fish swimming activity. However, by making assumptions of simplified fish swimming patterns (e.g. with the fish swimming in circular motion against the current direction at their preferred speed) and based on recent experimental measurements, cf. (Gorle et al., 2018), one may include the effects related to fish biomass, making the CFD results more accurate.

3.2.2. Existing flow models

In the AQUAEXCEL2020 project (Alver, 2020), the CFD code ANSYS Fluent was used to provide numerical simulations of the stationary flow in geometries corresponding to three different tank designs located at:

1. VURH Vodnany: circular 1.4 m^3 tanks
2. HCMR Heraklion: circular 0.55 m^3 tanks
3. NOFIMA Sunndalsøra: octangular 1.8 m^3 tanks

All calculations were performed using a Reynolds-averaged Navier-Stokes equation system and the Intermittency k-omega SST turbulence model. The simulation data was made available through the Virtual Laboratory, but visualizations were also provided in the report (Alver, 2020). We include the visualizations here in the form of velocities in horizontal sections for the VURH tank (Figure 2), streamline visualization for the HCMR tank (Figure 3), and horizontal sections for the NOFIMA tank (Figure 4).

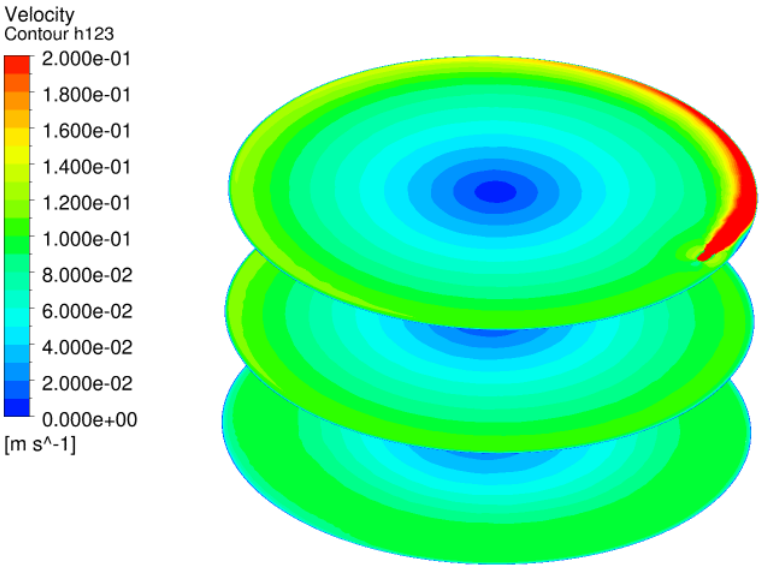

Figure 2: Example of velocity flow field in VURH tank, computed using Ansys Fluent. The figure shows velocity contours in three planes above the tank bottom. The upper contour plot shows the higher velocities originating from a water inlet. The other dominating features are a lower current velocity closer to the centre of the tank, and a slight reduction of current near the tank wall except those areas affected by the water inlet.

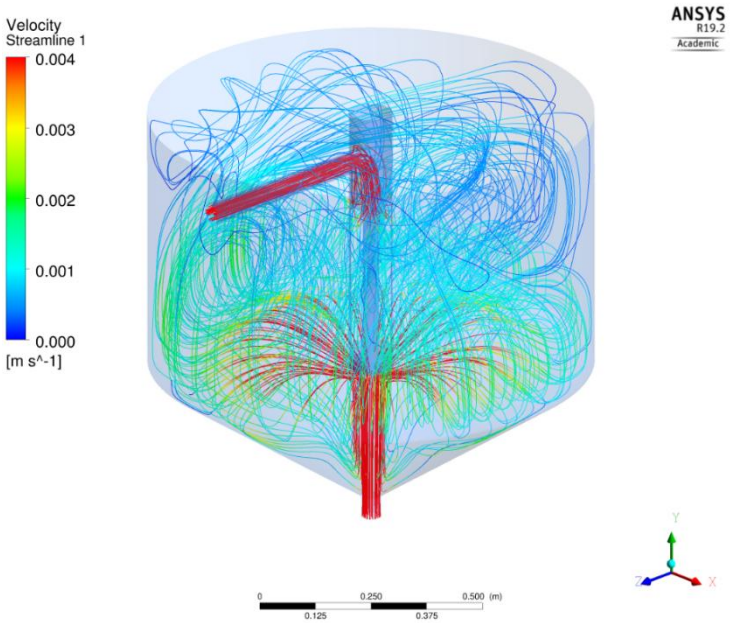

Figure 3: Streamlines illustrating the flow pattern in the HCMR tank.

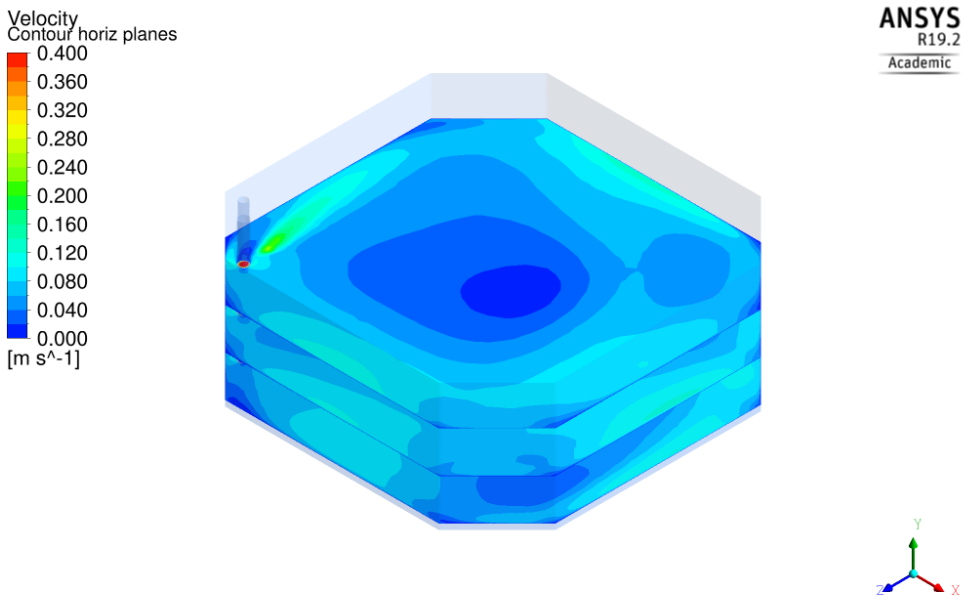

Figure 4: Example of velocity flow field in NOFIMA tank, computed using Ansys Fluent. The figure shows velocity contours in three planes above the tank bottom.

3.2.3. Simulation of new tank designs

Choice of tank designs

The existing model simulations covered sizes from 0.55 m^3 up to 1.8 m^3. Considering the reported range of tank sizes, the smallest and largest sizes are not represented by existing simulations. The tank systems smaller than the 0.55 m^3 tanks are typically used for fish larvae, plankton or for specialized experiments, often set up with low current speeds, meaning it will be challenging to model clear flow patterns. Therefore, the selection of new tank designs was made to expand the range towards larger systems. The following two tank designs were chosen:

1. HCMR: octangular 10 m^3 tanks
2. INRAE: circular 22 m^3 tanks

Detailed drawings of the tank designs were obtained from the HCMR (see two examples in Figure 5 and Figure 6) and INRAE (see examples in Figure 7 and Figure 8) labs to facilitate model setup.

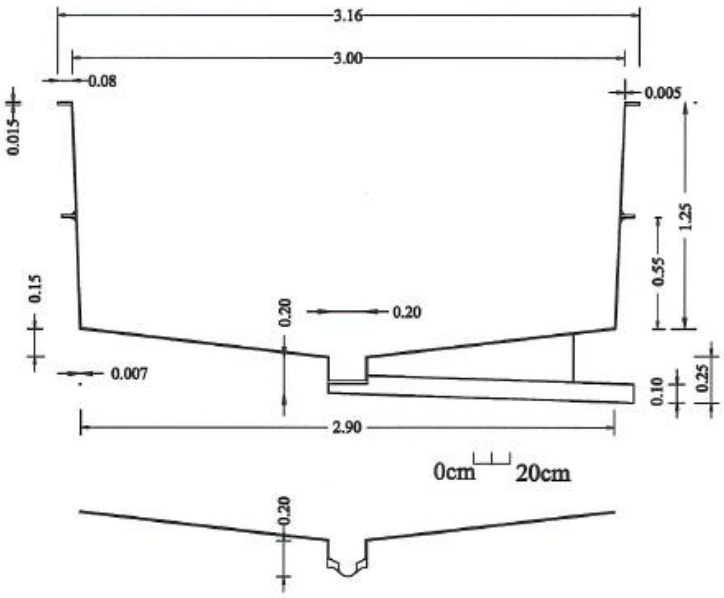

Figure 5: Side view of HCMR tank with metrics. Internal width is 3 m, and the water outlet is in the bottom centre. In the centre (not shown in the figure) is a vertical cylinder with large holes wrapped in mesh reaching from the bottom to the top, serving as a filter for the outlet water.

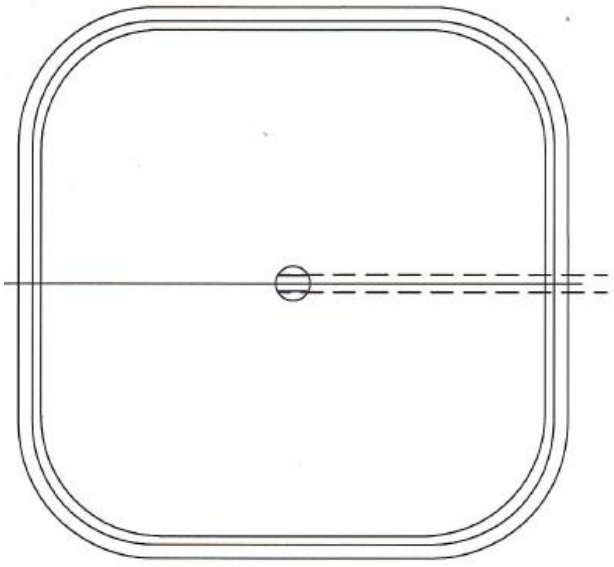

Figure 6: Top view of HCMR tank. The tank is rectangular with rounded corners.

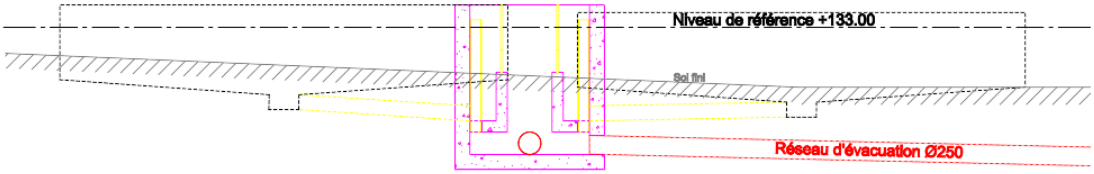

Figure 7: Side view of INRAE tank. Two tanks are shown side by side in the figure, along with the outlet arrangement. The water depth near the outer edges is approximately 79 cm.

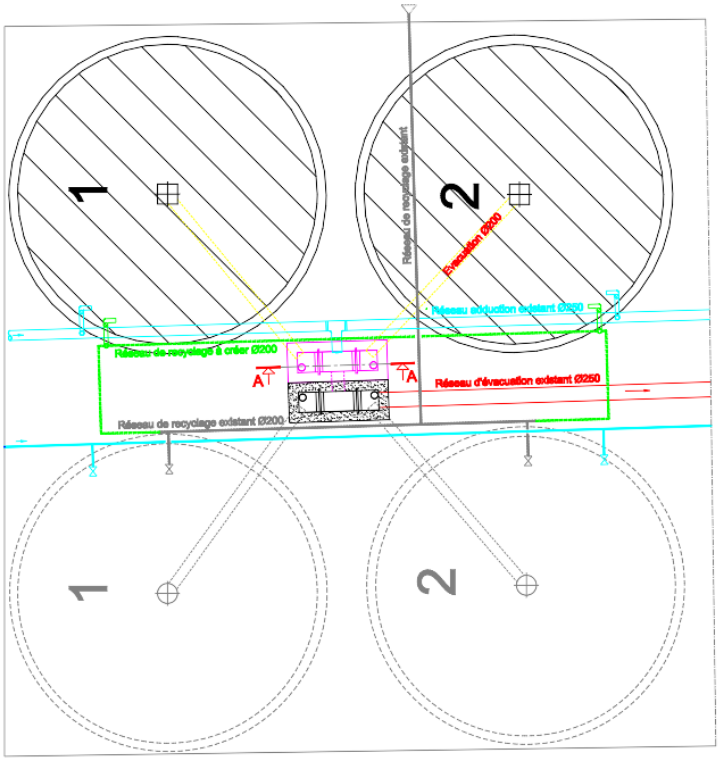

Figure 8: Top view of INRAE tank. Internal diameter is 6.03 m, and the water outlet is in the bottom centre.

Flow simulations in Fluent

Model grids for Fluent were created using Ansys SpaceClaim 3D modelling software[1], producing grids with around 7.3 million points for the HCMR system, and around 13.9 million points for the larger INRAE system. CFD simulations were done using Ansys Fluent 2022 R1. As in the AQUAEXCEL2020 simulations, all calculations were performed using a Reynolds-averaged Navier-Stokes equation system and the Intermittency k-omega SST turbulence model. The simulations were set up to estimate steady state flow fields.

A total of 8 simulations were run, covering two variants of the two tank designs, and minimum and maximum inlet flow rates (Table 1). The difference between the "original" and "modified" tank designs were in the inlet geometries; in the modified setups the inlets were designed to distribute the water flowing into the tanks more evenly in the vertical dimension in order to facilitate a clearer current pattern with stronger currents near the bottom. Such an arrangement can potentially increase the self-cleaning capacity of the tanks.

Table 1: Overview of CFD simulations

SIMULATION #	TANK DESIGN	MODEL VARIANT	# GRID POINTS	FLOW RATE	FLOW (M^3/H)
1	HCMR 10 m^3	Original	7,294,473	MIN	5
2	HCMR 10 m^3	Original	7,294,473	MAX	15
3	HCMR 10 m^3	Modified	7,389,947	MIN	5
4	HCMR 10 m^3	Modified	7,389,947	MAX	15
5	INRAE 22 m^3	Original	13,852,945	MIN	10
6	INRAE 22 m^3	Original	13,852,945	MAX	35
7	INRAE 22 m^3	Modified	13,999,954	MIN	10
8	INRAE 22 m^3	Modified	13,999,954	MAX	35

[1] https://www.ansys.com/products/3d-design/ansys-spaceclaim

Post processing of simulation output

To facilitate inclusion of flow fields in the Virtual Laboratory, the Fluent output needs to be interpolated from the CFD model's unstructured grid onto a regular grid. A Python application has been developed for this purpose. The application performs the following operations:

1. Read the ASCII output file from Fluent containing current vector components at all grid centre positions. As the high number of cells in the unstructured grid makes the interpolation process very computationally demanding, subsample the data by including only every 10^{th} grid cell.
2. Define a regular 250x250x150 grid encompassing all (x, y, z) locations in the simulation domain.
3. Using the **griddata** function of the **scipy.interpolate** package, interpolate the components of the flow field onto the defined grid.
4. Store the interpolated current vectors in NetCDF format.

See Appendix A for the full source code of the Python application.

If users conduct new Fluent simulations to assess the flow fields of new types of tanks, the Python code can be used to produce similar NetCDF files that can be used with the Virtual Laboratory. This requires ASCII output to be stored for cell centres for the steady state field. Minor adjustment to the Python code may be required if the ASCII output is differently configured.

3.2.4. Turbulence

Fluent provides values for Turbulent Kinetic Energy (TKE), which is the mean kinetic energy per unit mass associated with eddies in turbulent flow. TKE is relevant for assessing the overall level of turbulent motion in a tank, and has an impact on how water and particles move and on their average residence time.

3.2.5. Simulations of residence time distribution

Residence time distribution (RTD) is a measure of how long dissolved material or particles stay in a tank before getting transported out. The RTD for a certain system can be estimated based on the modelled 3D flow fields. Using an approach similar to that of (Papáček et al., 2020), we estimate RTD by initializing a large number of particles within a tank and simulating their motion due to gravity and hydrodynamic forces.. Particles are assumed independent, so no interaction between them is modelled. Once a particle reaches the outlet of the tank, it is registered as inactive, and the simulation is run until all or nearly all particles are inactive.

The principles of particle simulations in Fluent are described in the Ansys Fluent Theory Guide (Ansys Inc., 2021), but we will give some of the main equations here.

One of the core equations describes the force balance for a particle:

$$m_p \frac{d\vec{u}_p}{dt} = m_p \frac{\vec{u} - \vec{u}_p}{\tau_r} + m_p \frac{\vec{g}(\rho_p - \rho)}{\rho_p} + \vec{F}$$

Where m_p is the particle mass, $\vec{u}$ is the flow velocity, $\vec{u}_p$ is the particle velocity, ρ is the fluid density, ρ_p is the density of the particle, $\vec{g}$ is the gravitational acceleration, $\vec{F}$ is an additional force, $m_p \frac{\vec{u}-\vec{u}_p}{\tau_r}$ is the drag force with τ_r being the particle relaxation time, which is calculated based on fluid viscosity, particle diameter and the relative Reynolds number.

The additional forces in $\vec{F}$ include two elements that are relevant for particles with densities not much higher than the density of the water. First, *added mass* accounts for the force required to accelerate the fluid surrounding the particle. Second, an additional force arises due to the pressure gradient in the fluid. Refer to Ansys Inc. (2021) for details of how these are calculated.

Turbulence will act to disperse particles, and in a turbulent flow there will always be turbulent motion below the spatial scales resolved by the model. This needs to be accounted for by adding random perturbations of particles. This is done by adding a random walk term to particles, tuned according to the estimated turbulence of the flow field.

The particle equations are integrated using Fluent's default setting of automated tracking scheme selection, using *trapezoidal* integration as the high order scheme and *implicit* as the low order scheme.

To investigate residence times for the 8 simulation cases, two sets of particle simulations were run. First, neutrally buoyant particles were simulated to measure water retention time. Second, solid particles with a diameter of 0.5 mm and density of 1150 kg/m3 were simulated to measure particle residence time. Simulations ran a variable number of iterations, terminating when a certain percentage of particles had left the system, or when reaching the maximum of 1 000 000 iterations.

3.2.6. Validation study

For comparison with simulated flow fields, a set of measurements were run in one of the HCMR 10 m^3 tanks. The tank was filled with sea water but containing no fish. To ensure sufficient particular matter for doppler based measurements, a small amount of mud was added to the water periodically in small increments for the duration of the measurements.

Measurements were made for two cases: minimum and maximum inlet flow rate. For each case, measurements were made in a grid of 3 heights and 38 horizontal positions. The horizontal positions are shown in Figure 9.

Each inlet of the tank was set up with a perforated pipe around it that serves to reduce the speed of the inlet water (Figure 10). This practice is established for rearing small fish as it ensures sufficient water exchange without creating high speed areas around the inlet which could inhibit swimming and feeding.

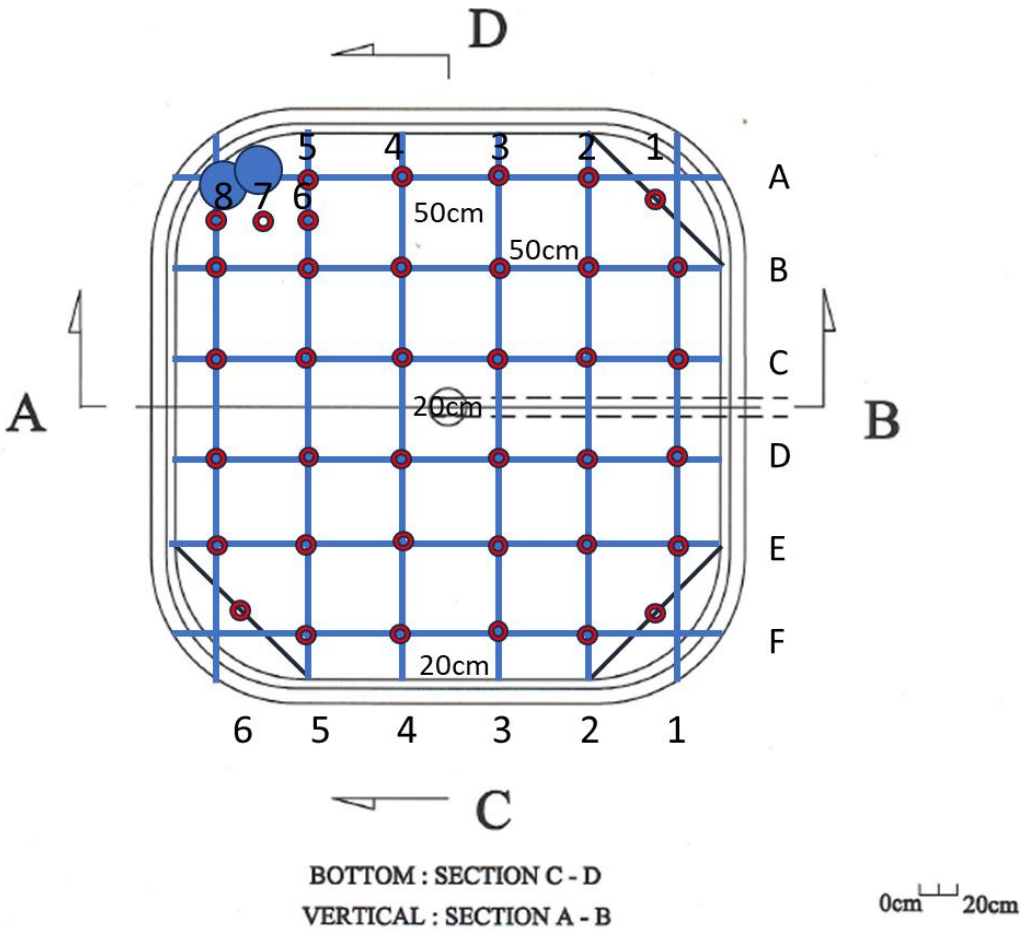

Figure 9: Overview of measurement positions in validation study. The blue circles indicate water inlet surrounded by a perforated pipe.

Figure 10: Photograph of the HCMR tank with the inlet arrangement using a current reduction device.

Measurements were made using a Nortek Vectrino velocimeter[2]. The Vectrino is an acoustic doppler based point sensor for turbulence and flow velocity. The sensor was moved sequentially between all measurement positions, with a 5-minute pause after each move to allow the flow field to settle back into steady state. As each measurement has some uncertainty, and there will be some turbulent variability in the flow, each measurement was made by recording current over a period of 10 minutes and averaging.

As the measurements cover three horizontal planes of the tank at a reasonable resolution, the average current vectors for each plane were interpolated over the entire horizontal plane to provide an estimate of the flow field in the plane.

[2] https://www.nortekgroup.com/products/vector-300-m

3.3. Flow fields in sea cages

Flow fields in sea cages have not been a focus of the AQUAEXCEL3 project, but for completeness we include here the description of the model that was established in the AQUAEXCEL2020 project.

In the case of cages, no established models exist to simulate currents as function of outside current and the activity of the fish, although many aspects of the flow in sea cages have been investigated (Klebert et al., 2013). The current outside the cage at a given location may be monitored using point or profiling current meters, and modelled using regional ocean models such as SINMOD (Slagstad and McClimans, 2005) or ROMS (Shchepetkin and McWilliams, 2005). The vertical current profiles observed at an aquaculture location depend on which processes dominate the dynamics at the location. Some of the relevant processes are tidal dynamics, wind induced currents and stratification caused by freshwater run-off. Aquaculture farms may generally be categorized according to the type of current and hydrography conditions they experience. In the Norwegian salmon industry, for instance, there are some sheltered fjord locations, with limited wind and waves, high stratification and mainly tidal currents and estuarine circulation, and more exposed locations with stronger wind and wave effects, less pronounced tidal currents and with current influenced by the Norwegian Coastal Current.

The current speed inside of the cage is dependent on outside current and the properties of the cage (Løland 1993). The outside current for each individual cage in a fish farm depends also on the cage's position, as the wake from upstream cages will affect the current speed. Cages deform in strong currents, making the dynamics more complicated (see Figure 11). Løland (1993) developed a method for calculating the current forces on a net structure and the resulting wake, including estimates of current inside the cage, and compares results to laboratory scale model test. An approximate inside current speed of 85% of the ambient current speed is found for a reasonable set of parameters. Endresen et al. (2013) used a net cage model implemented in SINTEF's FhSim modelling framework (Reite et al., 2014) to estimate wake effects acting within an aquaculture net cage, comparing numerical estimates with experimental data. An approximate inside current speed of 80-85% of the ambient current speed was found.

As with CFD modelling of tanks, the effect of the fish is difficult to account for. Depending on the biomass and density of fish, and their swimming pattern, the fish may cause an attenuation of current speeds, may modify current directions and can potentially add to the turbulent motions of the water (Klebert et al., 2013). Models describing the current flow field inside net cages in more detail may become available through ongoing research, but at present the best approach is to do a simple parameterization based on the ambient current profile to estimate the flow field inside.

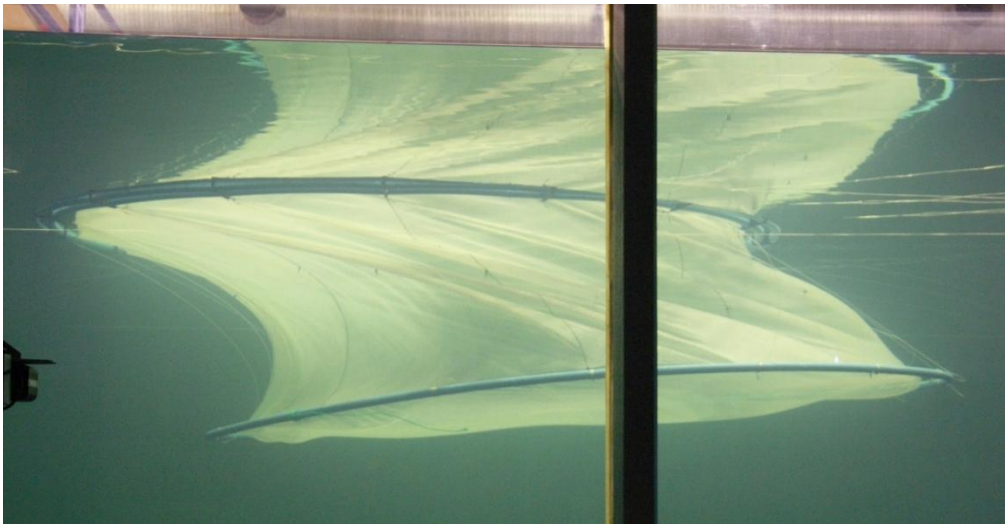

Figure 11: Photograph of downscaled net cage model in a laminar current field (Photo: SINTEF Ocean).

3.4. Technical implementation

3.4.1. Model functionality

In the case of tanks, due to the computational cost, computing a flow field based on user inputs is time consuming and requires high performance hardware. Therefore, it is not practical to run the current model on demand through the virtual laboratory web interface. The solution is to provide precomputed flow fields for the available selection of tank designs and operating conditions. These precomputed fields are stored in NetCDF files. As long as the output is stored or convertible to a suitable format, any CFD model may be used for this purpose. It is also possible for users of the VL to add their own simulation data for new tank designs, as long as they can be converted into the appropriate NetCDF format using a conversion script like the one given in this report.

In the case of cages, the flow field is estimated based on outside current conditions in the form of vertical profiles of current direction and speed. The user will be able to either choose and adjust typical profiles, or input their own. The vertical current profile to use will be written in NetCDF format for access by the model.

In either case, the key functionality of the flow field model component is to provide information about the water current in the tank or cage. The model provides two sets of outputs – one that contains 3D current components (e.g. current upwards, towards the east and towards the north) at a requested position, and another that provides overall descriptive values characterizing the flow field.

3.4.2. Model interface

The initialization of the model requires a path to a data file in NetCDF format containing the precomputed flow field or current profile. This file will be opened upon startup of the model, and will be accessed through the course of the simulation to extract the information needed to compute the requested model output values. The model automatically recognizes whether the file contains a tank flow field or a cage profile, and configures itself accordingly.

Table 2 lists the initialization parameters required by the model. This list may be expanded in future versions of the model.

Table 2: Model initialization parameters

Name	Type	Data type	Description
filename	Input	String	Path to NetCDF file containing flow field or current profile
tidal	Input	Numerical	0 to disable tides, 1 to enable

Input values

The input values to the model are the x, y and z coordinates of a requested position (listed in Table 3).

Table 3: Input values

Name	Type	Unit	Description
xPos	Input	m	Requested position along the *x* axis
yPos	Input	m	Requested position along the *y* axis
zPos	Input	m	Requested position along the *z* axis

Output values

The module outputs the current vector for the requested position, as well as a selection of descriptive values for the flow field. Output values are listed in Table 4.

Table 4: Output values. Values marked with (*) are only available if they can be read or calculated from the input NetCDF file.

Name	Type	Unit	Description
xVel	Output	m/s	Current speed along the *x* axis
yVel	Output	m/s	Current speed along the *y* axis
zVel	Output	m/s	Current speed along the *z* axis
vAvg	Output	m/s	Average speed
vMin	Output	m/s	Minimum speed
vMax	Output	m/s	Maximum speed
minX	Output	m	X position of minimum speed
minY	Output	m	Y position of minimum speed
minZ	Output	m	Z position of minimum speed
maxX	Output	m	X position of maximum speed
maxY	Output	m	Y position of maximum speed
maxZ	Output	m	Z position of maximum speed
*avgTke**	Output	J/kg	Average turbulence kinetic energy
*minTke**	Output	J/kg	Minimum turbulence kinetic energy
*maxTke**	Output	J/kg	Maximum turbulence kinetic energy
*minTkeX**	Output	m	X position of minimum TKE
*minTkeY**	Output	m	Y position of minimum TKE
*minTkeZ**	Output	m	Z position of minimum TKE
*maxTkeX**	Output	m	X position of maximum TKE
*maxTkeY**	Output	m	Y position of maximum TKE
*maxTkeZ**	Output	m	Z position of maximum TKE

3.4.3. Integration into Virtual Laboratory

The flow field model component is written in C++ and packaged both as a Functional Mock-up Unit (FMU), and as a dynamic library (DLL). The model utilizes the NetCDF 4 library[3] which provides functionality for reading and writing NetCDF files. At startup, the FMU opens the NetCDF file and reads the metadata defining the grid or the vertical profile. The NetCDF format allows for metadata describing units and the geometry of the data contained. Provided the input NetCDF file is well formatted, no additional information is needed for the model to relate the flow field to the tank geometry. The layout of a NetCDF file can be shown using the CDL (network Common data form Description Language) format, in which file dimensions and variables with attributes are listed. The following listing shows the CDL of a file containing a three-dimensional current flow field (given as components *u*, *v* and *w*), with metadata providing grid and variable units:

```
netcdf datafile {
dimensions:
        xc = 400 ;
        yc = 400 ;
        zc = 200 ;
variables:
      float xc(xc) ;
            xc:units = "m" ;
      float yc(yc) ;
            yc:units = "m" ;
      float zc(zc) ;
            xc:units = "m" ;
     float u(zc, yc, xc) ;
            u:units = "m/s"
     float v(zc, yc, xc) ;
            v:units = "m/s"
     float w(zc, yc, xc) ;
            w:units = "m/s"
}
```

In the case of net cages, the vertical profile is read upon startup, and stored in memory. In the case of tanks, no further data is read upon initialization of the model. All output values, except the current vector for a requested position, are calculated upon initialization of the FMU and stored for output in all subsequent time steps.

[3] NetCDF libraries are open source and can be downloaded at https://www.unidata.ucar.edu/downloads/netcdf/index.jsp.

When accessing the flow module as a DLL, the interface is defined through the header file reproduced in Appendix B.

Calculation of current vector

When the Functional Mock-up Interface (FMI) master calls for the model to advance to the next time step, new *xPos*, *yPos* and *zPos* values are provided. In the case of net cages, the *zPos* value is used to extract the appropriate current vector from the vertical profile, and the vector components *xVel*, *yVel* and *zVel* are returned. In the case of tanks, the appropriate data cell is found based on the given coordinates, and the current velocity of the cell is read from the NetCDF file. If the file provides vector components, these are returned directly. If the file provides axial, radial and vertical velocities, vector components are calculated from these and returned.

Calculation of current descriptor values

To calculate current descriptor variables, the entire flow field is read from the NetCDF file, and the appropriate calculations are performed, such as finding the minimum, mean and maximum speeds. All of this is done at model initialization, and no further calculations are done when the model advances in time steps.

Module interactions

When setting up an experiment in the VL, the user will make selections that determine the setup of the flow field model:

- In the case of tanks, the user will choose which supported tank design to use
- In the case of sea cages, the user will choose the type of location (fjord or exposed), high or low current scenario and to activate/deactivate tidal variations

Based on the experiment setup, the flow field model will provide the defined set of output values. If another model module provides the *xPos*, *yPos* and *zPos* input values, it may read back the outputs *xVel*, *yVel* and *zVel*.

The flow module is most tightly coupled with the behaviour module. As the behaviour module requires the lookup of the flow at a large number of positions per time step, it is not convenient to pass the information through the FMI interface. Instead, the flow module is linked directly to the behaviour module as a dynamic library, meaning that the values can be requested through internal C++ function calls.

As part of the model output summary, the VL will display and visualize key outputs from the flow field model.

4. Results and Discussion

4.1. Flow fields in tanks

4.1.1. Flow patterns

The steady state flow fields in the CFD simulations are illustrated in Figure 12 and Figure 13 for the HCMR system, and in Figure 14 and Figure 15 for the INRAE system. For each system, two perpendicular transects have been chosen, and the figures show the current velocities along those two transects for each simulation.

For the HCMR tank, high flow gives higher current speeds than low flow, both near the water inlet and in the whole tank volume. The system with modified inlet design clearly exhibits stronger current speeds. In the original design water flow rapidly downwards into the tank, while in the modified design it exits a vertical pipe through holes distributed over the tank's entire depth. The modification leads to a stronger and more directed flow in the tank volume.

For the INRAE tank, high flow also gives higher current speeds than low flow, but speeds are still relatively slow at maximum flow in the original system. The modified system directs the inflow through holes in the inlet pipe along the tank's depth, and sets up a clear circular motion in the tank with quite high speeds near the outer edge of the tank.

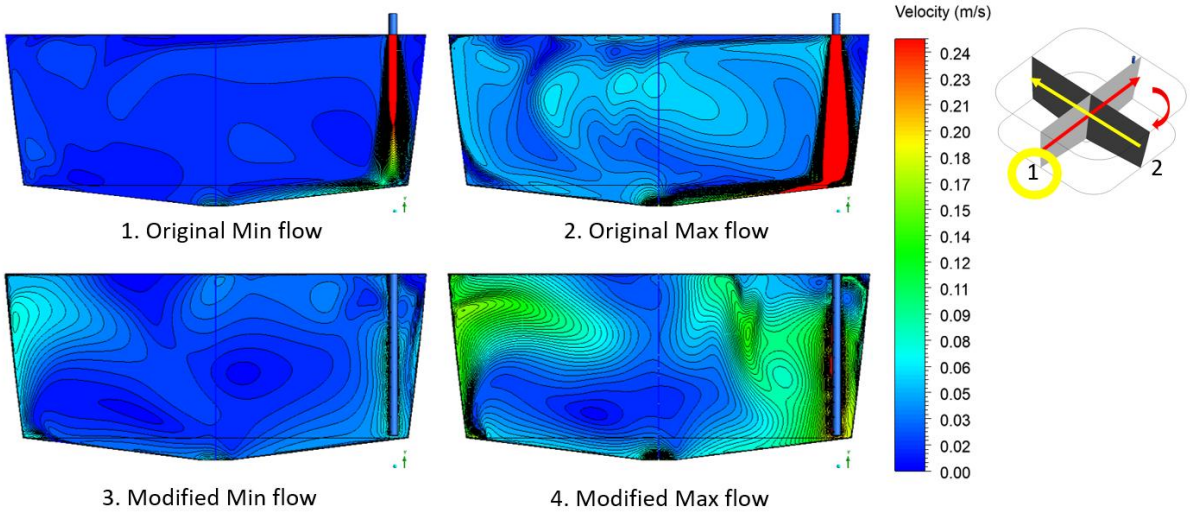

Figure 12: Flow velocities in HCMR system (simulations 1-4) along transect 1.

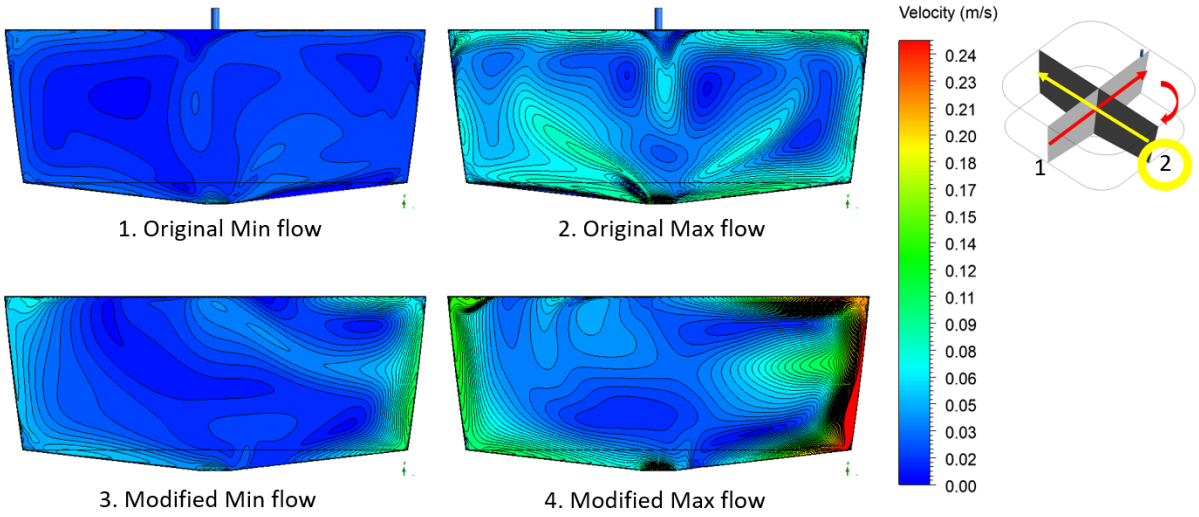

Figure 13: Flow velocities in HCMR system (simulations 1-4) along transect 2.

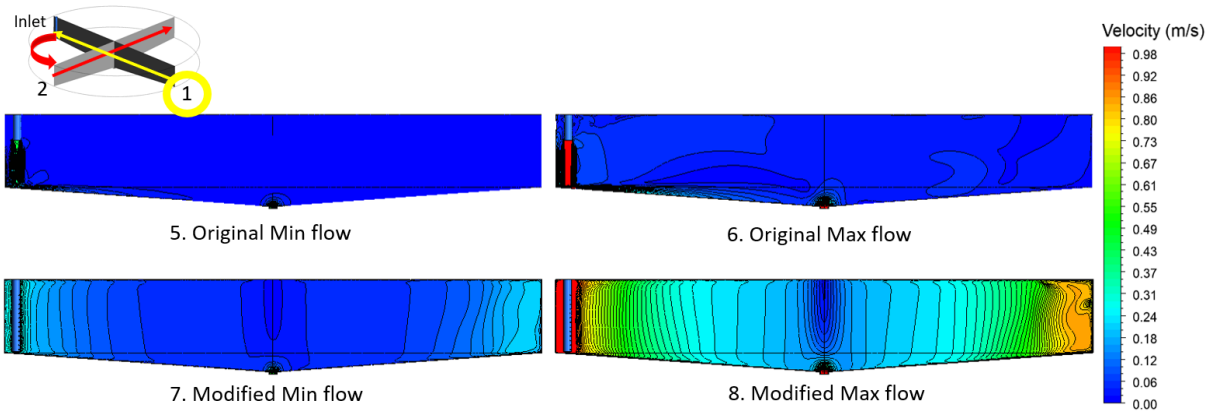

Figure 14: Flow velocities in INRAE system (simulations 5-8) along transect 1.

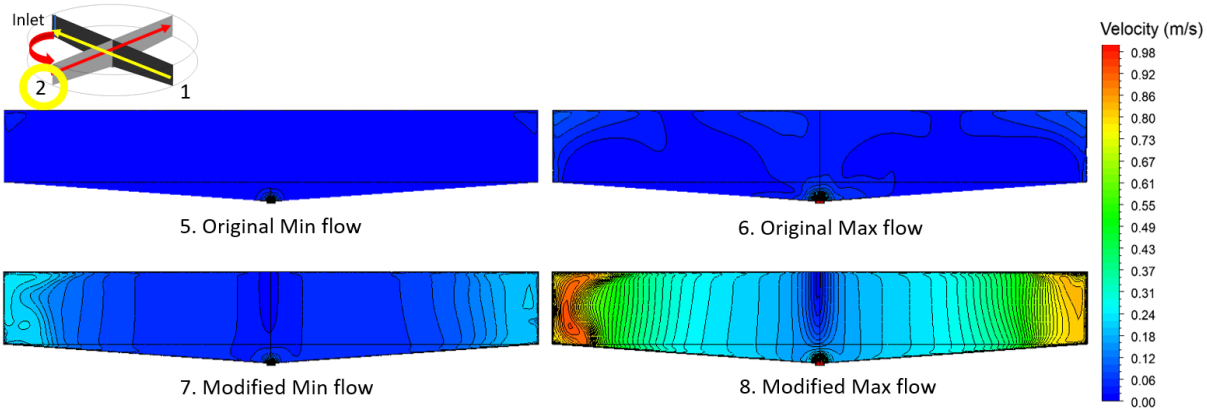

Figure 15: Flow velocities in INRAE system (simulations 5-8) along transect 2.

4.1.2. Turbulence

Figure 16 shows the calculated TKE for simulation 1 (HCMR original design with minimum flow) in a reference plane. As indicated in the figure, turbulence is strongest near the outlet in the bottom centre, and generally high near the bottom, in the regions near the edges (except in a boundary region very close to the edges) and near the surface. Figure 17 shows the corresponding values for simulation 2 (HCMR original design with maximum flow). The relative distribution of high and low turbulence zones is somewhat similar to simulation 1, but the higher flow rate leads to significantly higher TKE values throughout the tank.

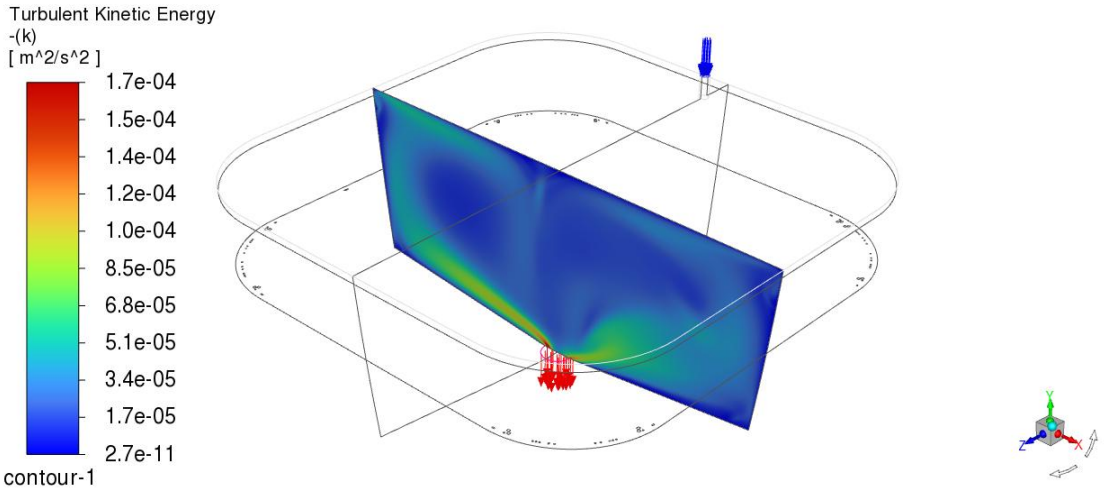

Figure 16: Turbulent kinetic energy for simulation 1 (HCMR original design with minimum flow) in a reference plane.

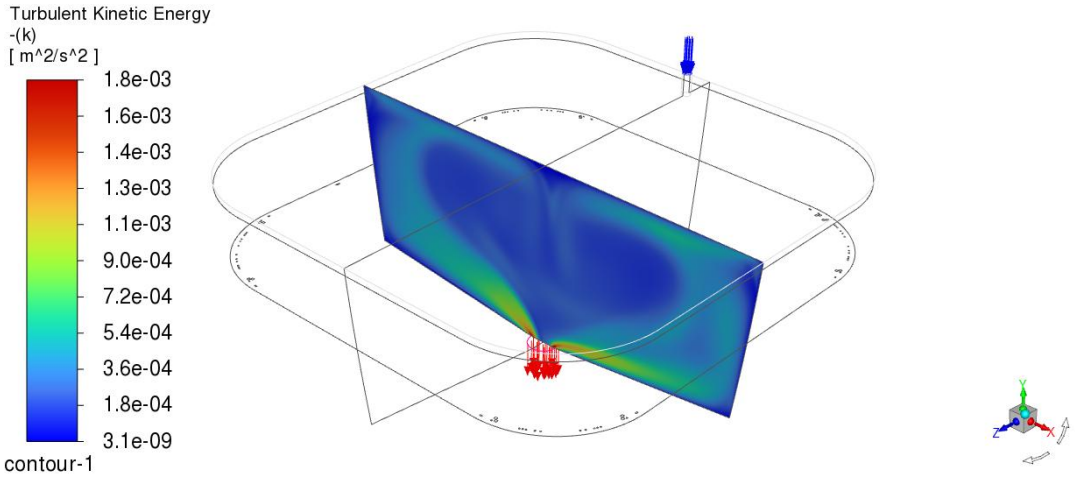

Figure 17: Turbulent kinetic energy for simulation 2 (HCMR original design with maximum flow) in a reference plane.

Figure 18 and Figure 19 show TKE in reference planes for simulations 3 and 4 for the modified HCMR setup (minimum and maximum flow, respectively). These show significantly higher average TKE compared to the original setup both for minimum and maximum flow. The relative distributions of TKE values are also different, with the highest turbulence now being seen closest to the path of the inflowing water. The inflow in the modified setup has higher speed due to small holes in the perforated pipe, and therefore sets up a stronger circular flow in the tank. As shown in the figures, this also has a strong effect on the distribution of TKE values.

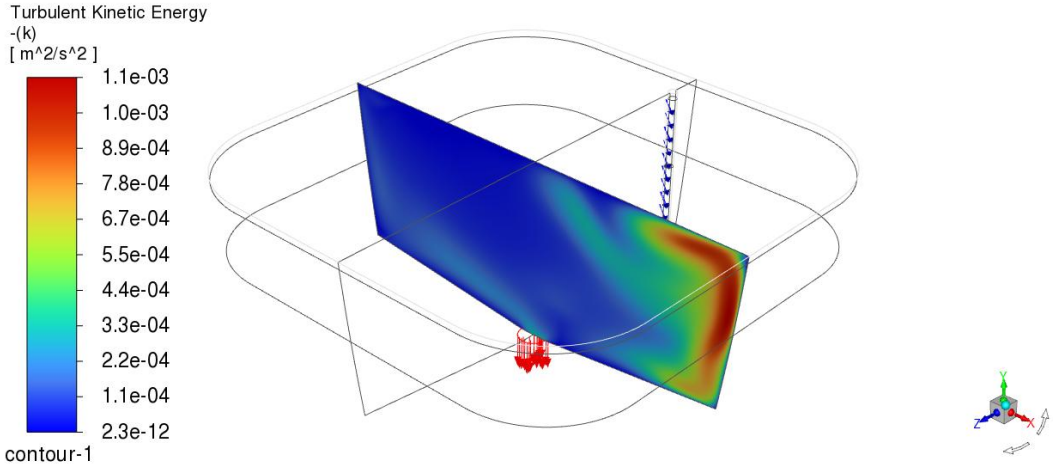

Figure 18: Turbulent kinetic energy for simulation 3 (HCMR modified design with minimum flow) in a reference plane.

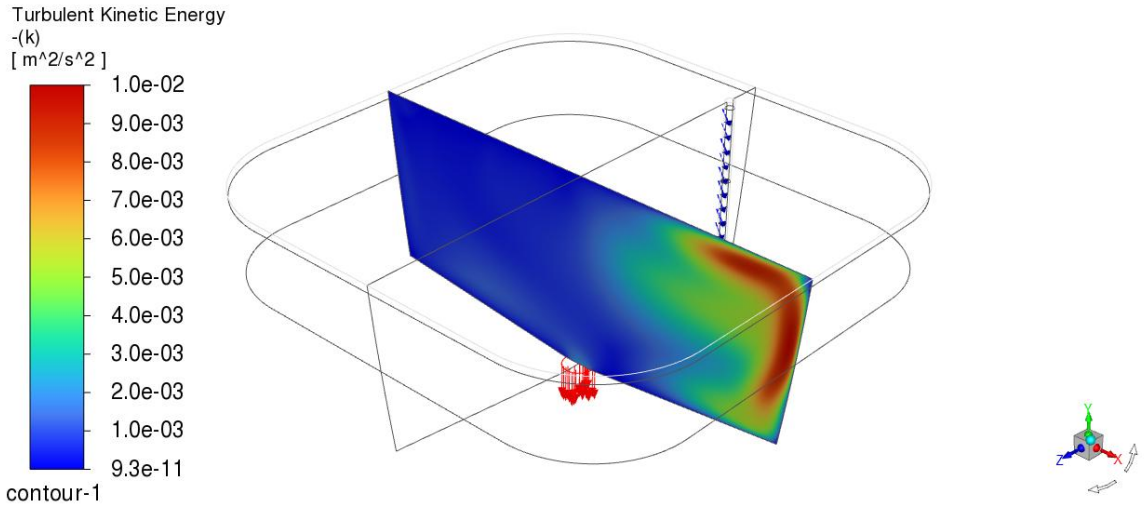

Figure 19: Turbulent kinetic energy for simulation 4 (HCMR modified design with maximum flow) in a reference plane.

Figure 20 to Figure 23 show the calculated TKE for simulations 5-8 (INRAE both designs, minimum and maximum flow) in a reference plane. In the original design, TKE is highest in the outer zone of the tank, as well as around the outlet. The modified design has higher average TKE values, and the increase is most pronounced near the outer edge of the tank on the side towards which the inlets are pointed. The increased inlet speeds set up a clear circular motion in the tank, and interaction between the high-speed water streams and the surroundings cause increased turbulence in this area.

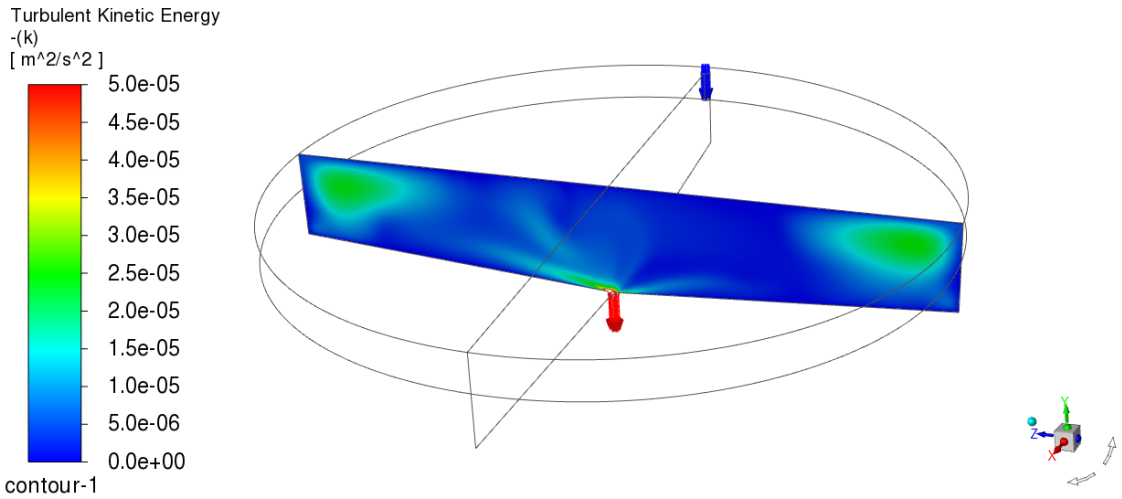

Figure 20: Turbulent kinetic energy for simulation 5 (INRAE original design with minimum flow) in a reference plane.

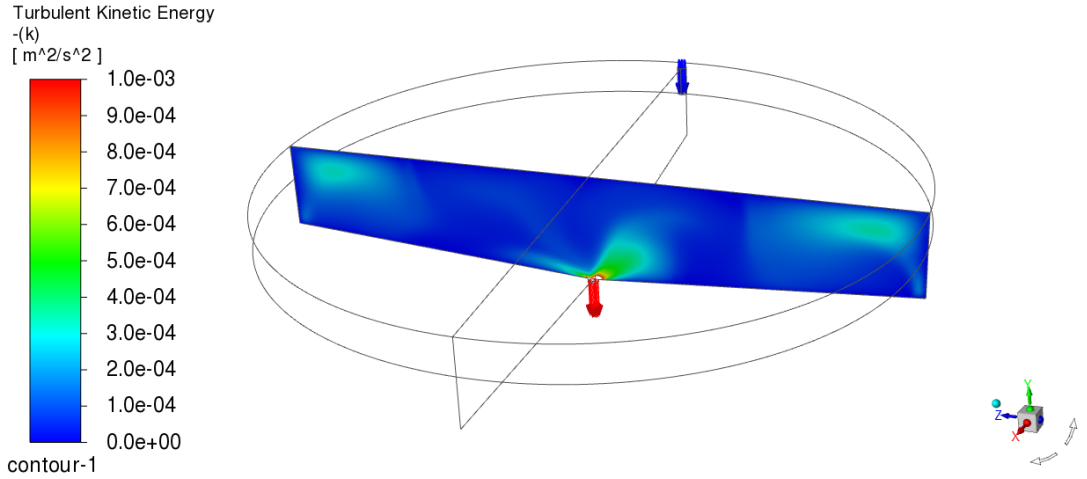

Figure 21: Turbulent kinetic energy for simulation 6 (INRAE original design with maximum flow) in a reference plane.

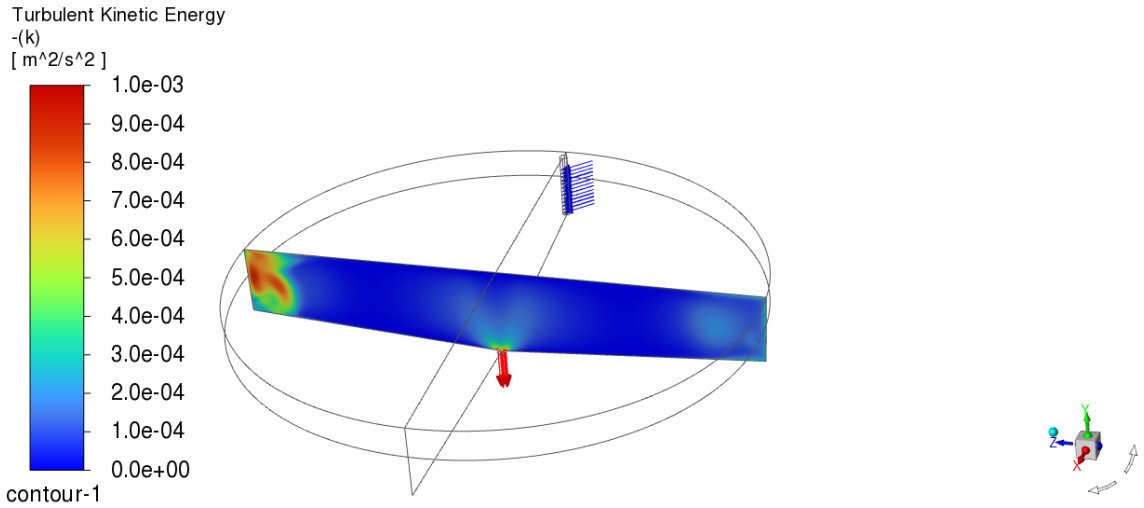

Figure 22: Turbulent kinetic energy for simulation 7 (INRAE modified design with minimum flow) in a reference plane.

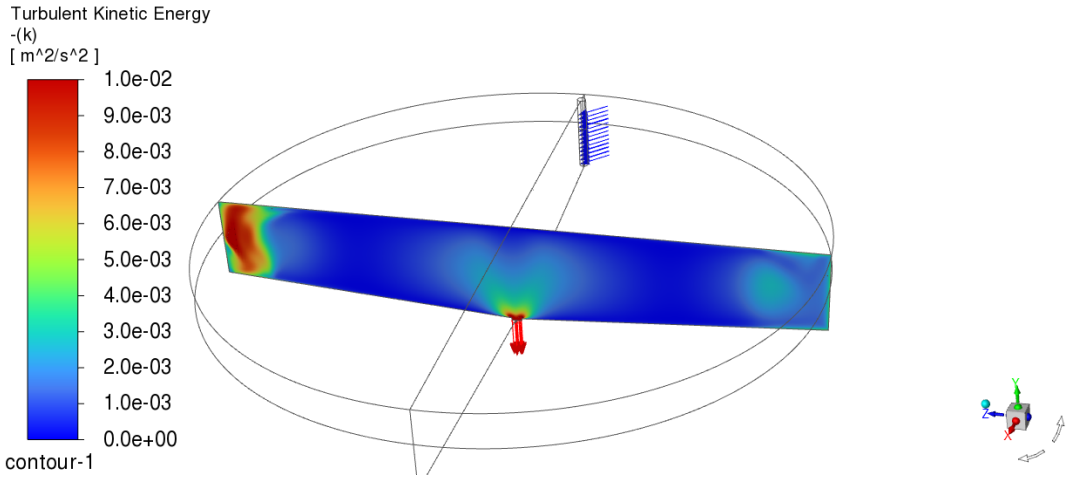

Figure 23: Turbulent kinetic energy for simulation 8 (INRAE modified design with maximum flow) in a reference plane.

Figure 24 shows the averaged TKE for the 8 simulations. The averages are not over the whole tank volume, but over the reference planes shown in the figures. We can see that the TKE values found are overall slightly higher in the HCMR tank compared to the INRAE tank. High flow rate leads to increased TKE, and for both systems the modified design leads to higher TKE values due to the increased speed of the inlet water.

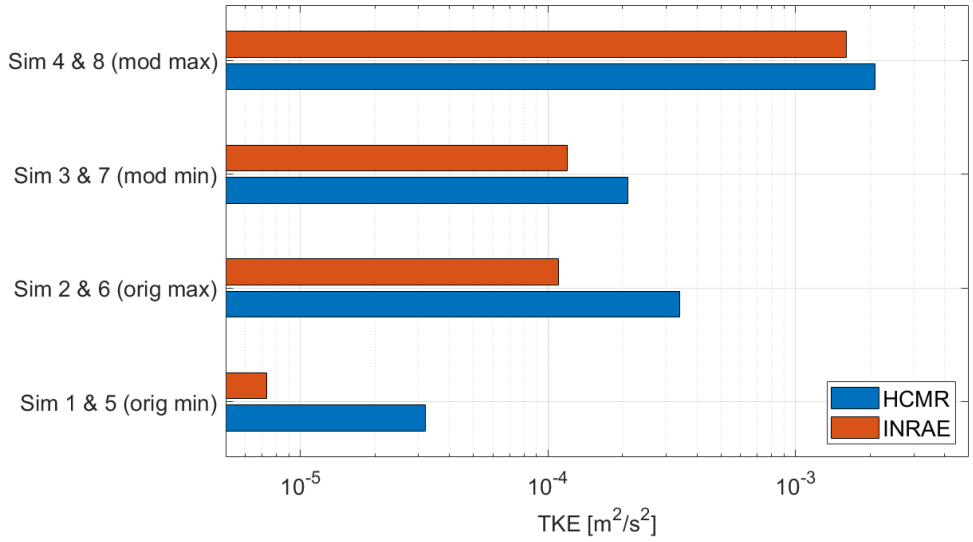

Figure 24: Average TKE for the 8 simulations.

4.1.3. Residence time distribution

Figure 25 shows the computed water and particle residence times for the HCMR system. For water retention, we see that average retention times are higher than the water exchange times (2 hours to exchange tank volume at the minimum flow 5 m^3/h, and 2/3 hour at the maximum flow 5 m^3/h). The initial paths of particles in the systems are indicated in Figure 26 for the original system and Figure 27 for the modified system. Comparing these figures, it is easy to see how the inlet setups lead to very different flow patterns in the tank. In the first case, water enters near the bottom and spreads out in all directions, while in the second case water enters at higher speed at the full range of depths and is directed sideways. The modified design promotes circular flow, as opposed to the original design.

There is little difference in water retention time between the original and modified systems. For particle retention, the time until 50% removal is actually higher at maximum flow, both for the original and modified systems. This is somewhat counterintuitive, but indicates that the higher turbulence levels at maximum flow may create water circulation zones keeping particles longer in the system. Times to 90% removal could not be computed, as particles stayed too long in the system. Particle simulation times were variable, and limited to a maximum of 1.000.000 iterations.

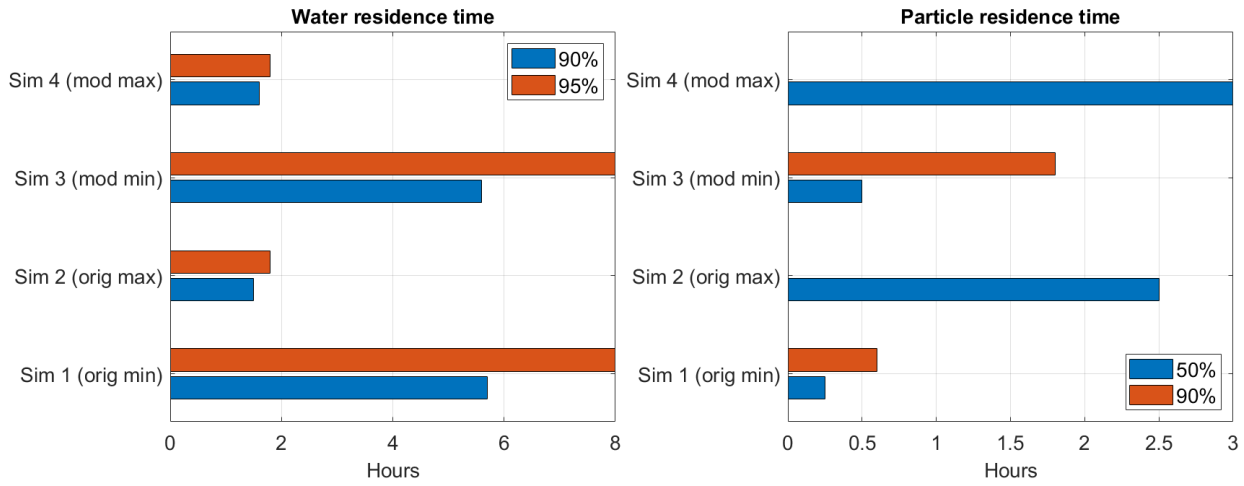

Figure 25: Water (left panel) and particle (right panel) residence times for the HCMR system. Percentages indicate the fraction of particles that have exited the system at the times shown. Note for particle residence times in simulations 2 and 4, particles remained in the system too long to compute times for 90% removal.

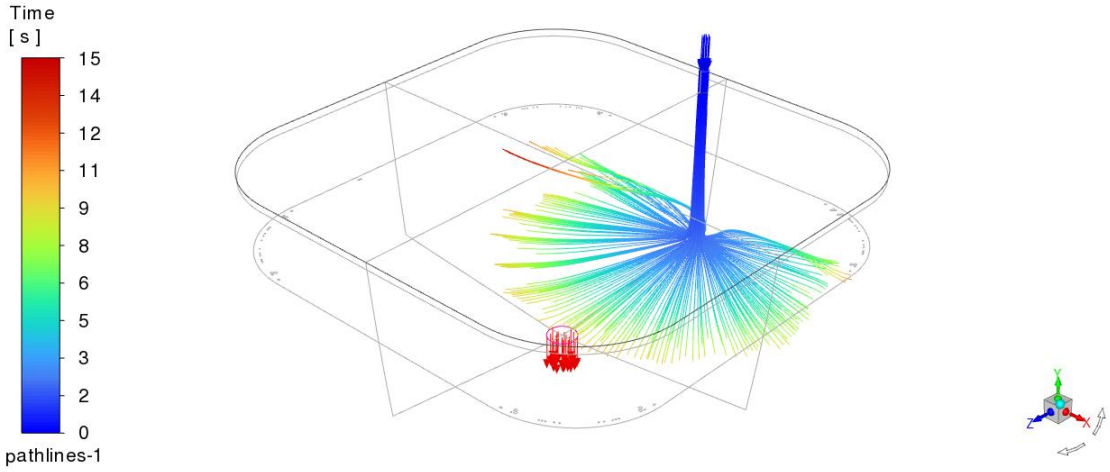

Figure 26: Particle traces for the first 15 seconds in HCMR tank with original design and maximum flow. The initial paths indicate that water enters near the bottom of the tank and flows out in all directions near the bottom before cycling into other parts of the tank.

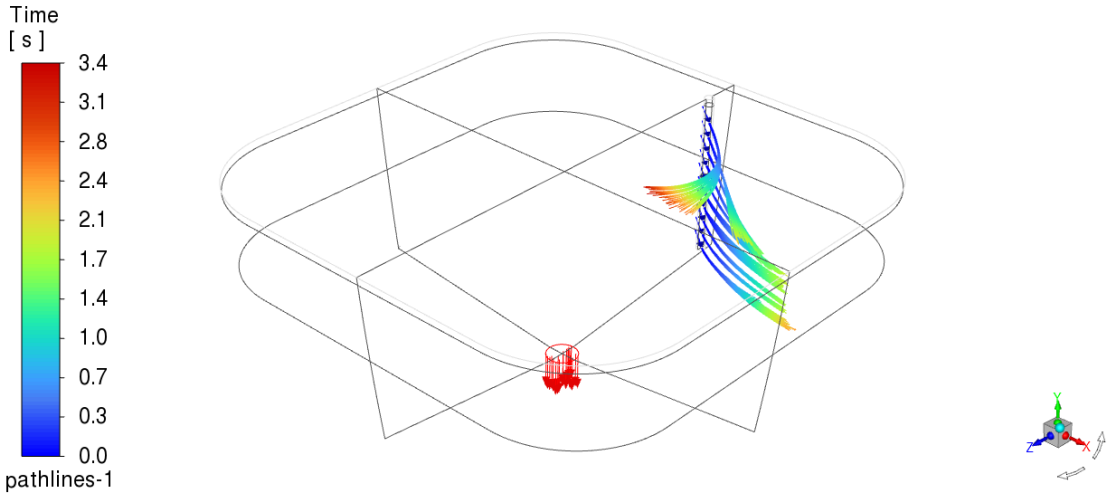

Figure 27: Particle traces for the first 3.4 seconds in HCMR tank with modified design and maximum flow. The initial paths indicate that with the modified inlet design, water enters near-horizontally at a range of depths, thereby setting up the stronger circulation pattern that was seen in the modified system.

Figure 28 shows the computed residence times for the INRAE system. As in the HCMR system, water retention times are longer than the water exchange times (2.2 hours to exchange tank volume at minimum flow, and 0.63 hours at maximum flow), and higher flow leads to shorter retention time. The modified system shows somewhat longer retention times than the original system. For particle residence, again residence time is higher at maximum flow than at minimum flow, although for the

INRAE system particles did not remain too long in the system for the residence time to be computed. The residence times are lower for the modified design compared to the original design.

The initial paths of particles in the systems are indicated in Figure 29 for the original system at maximum flow, and in Figure 30 for the modified system at minimum flow. As for the HCMR system, the inlet configuration leads to highly different initial particle patterns.

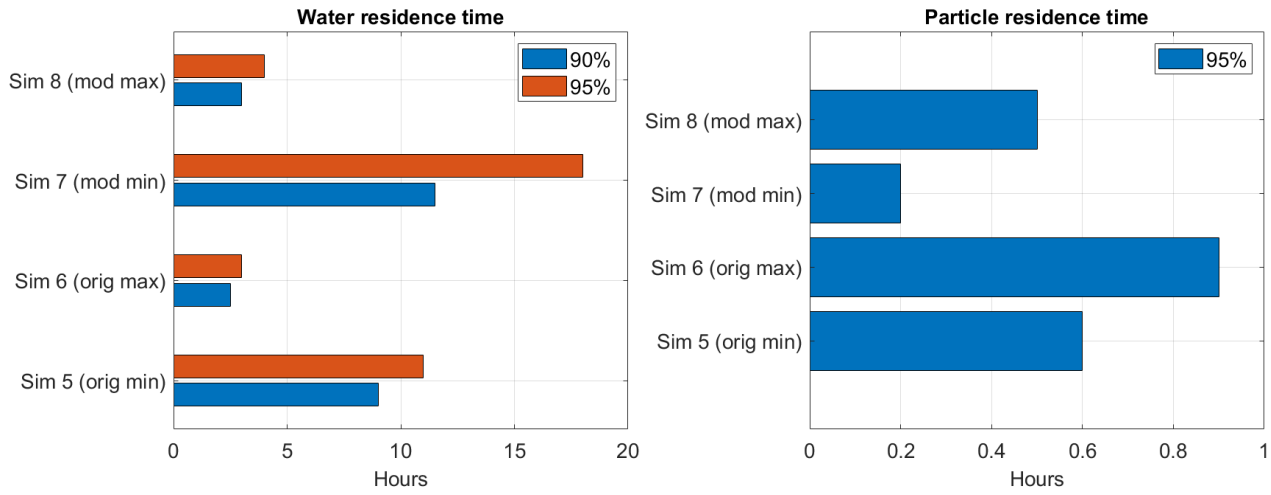

Figure 28: Water (left panel) and particle (right panel) residence times for the INRAE system. Percentages indicate the fraction of particles that have exited the system at the times shown.

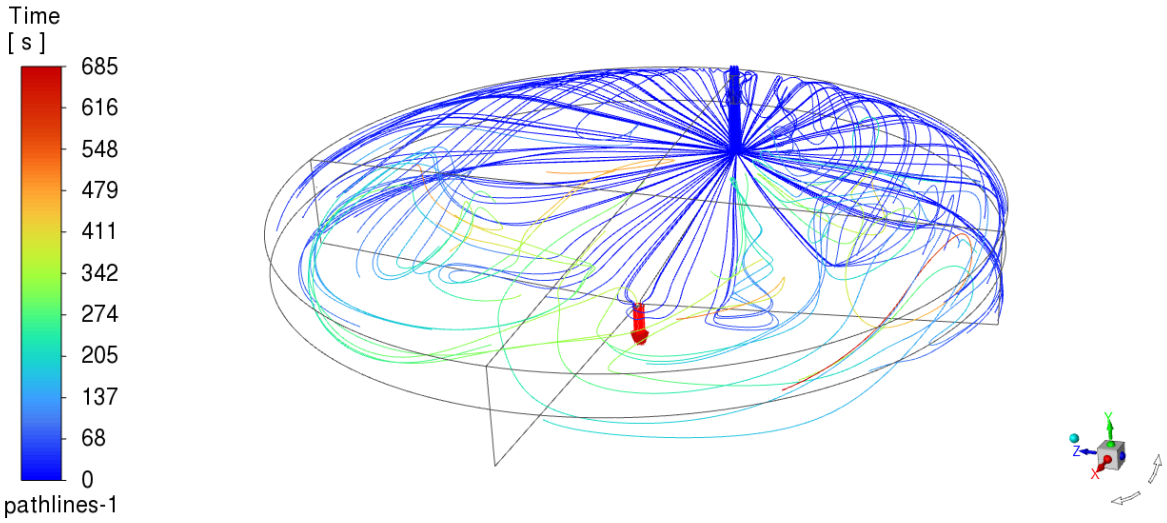

Figure 29: Particle traces for the first 685 seconds in INRAE tank with original design and maximum flow.

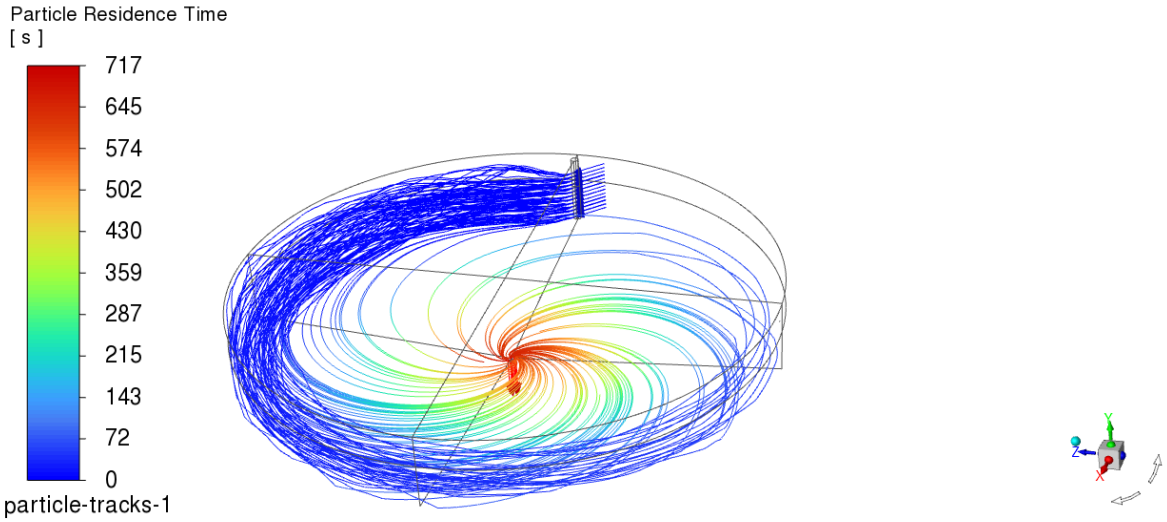

Figure 30: Particle traces for the first 717 seconds in INRAE tank with modified design and minimum flow.

4.1.4. Validation study

Figure 31, Figure 32 and Figure 33 show the interpolated current speeds and vectors in the lower, middle and upper planes, respectively, for the minimum flow scenario. Current speeds are below 0.01 m/s, without a clear pattern of elevated speeds near the water inlet. The patterns in current directions are also not clear, indicating that the water inlet does not set up a clear flow pattern in the tank.

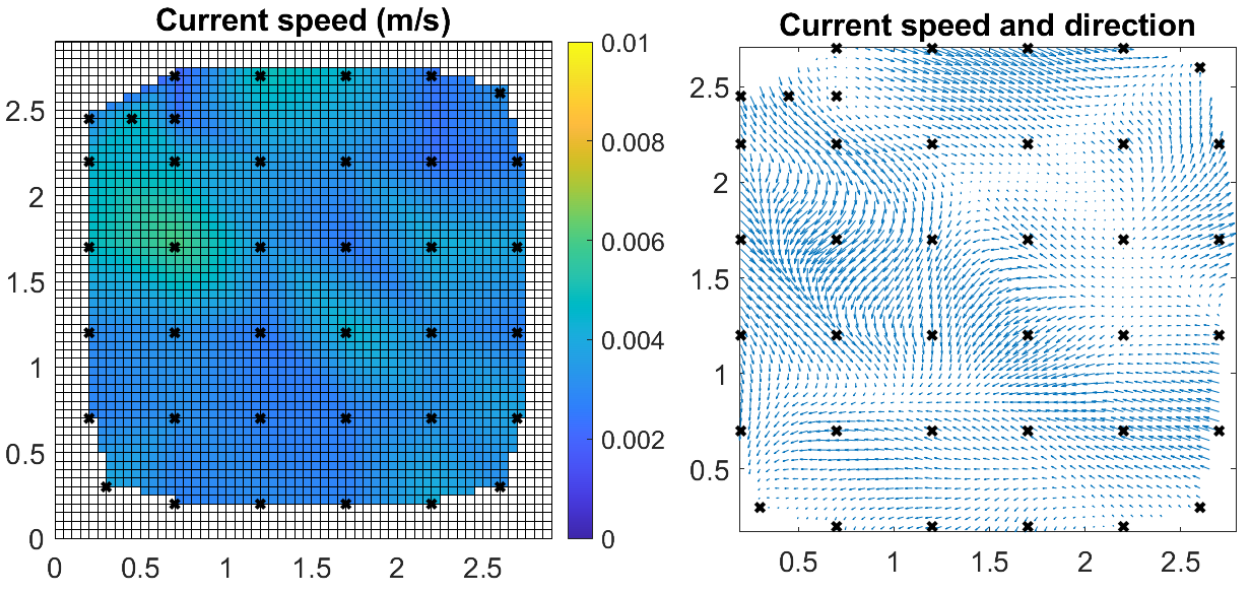

Figure 31: Interpolated current speeds and vectors in the lower plane at minimum flow.

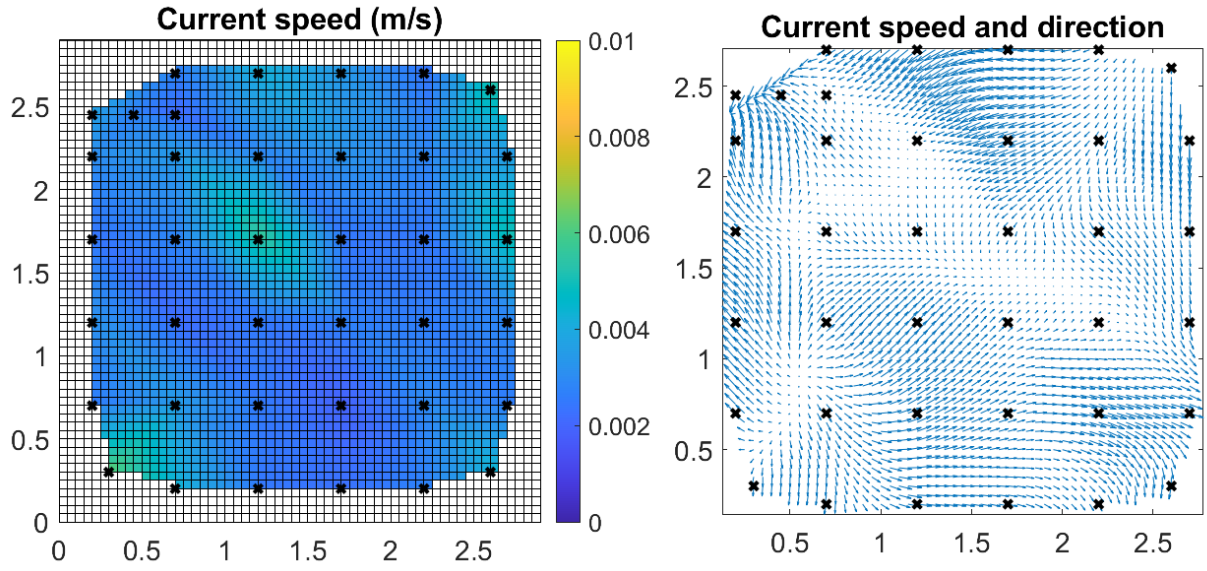

Figure 32: Interpolated current speeds and vectors in the middle plane at minimum flow.

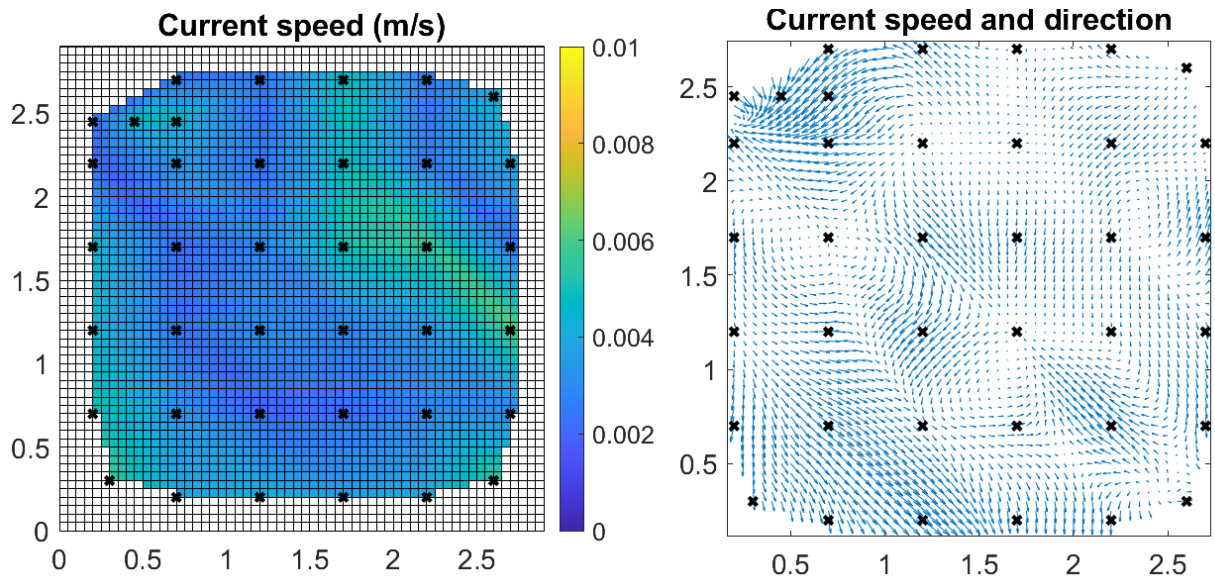

Figure 33: Interpolated current speeds and vectors in the upper plane at minimum flow.

Figure 34, Figure 35 and Figure 36 show the interpolated current speeds and vectors in the lower, middle and upper planes, respectively, for the maximum flow scenario. Current speeds are higher than in the minimum flow scenario, ranging up to 0.02 m/s, and there is now a clear pattern of elevated speeds near the water inlet, particularly in the lower plane. The patterns in current directions are still not very clear, indicating that despite the increased flow, the water inlet does not set up a very clear flow pattern in the tank.

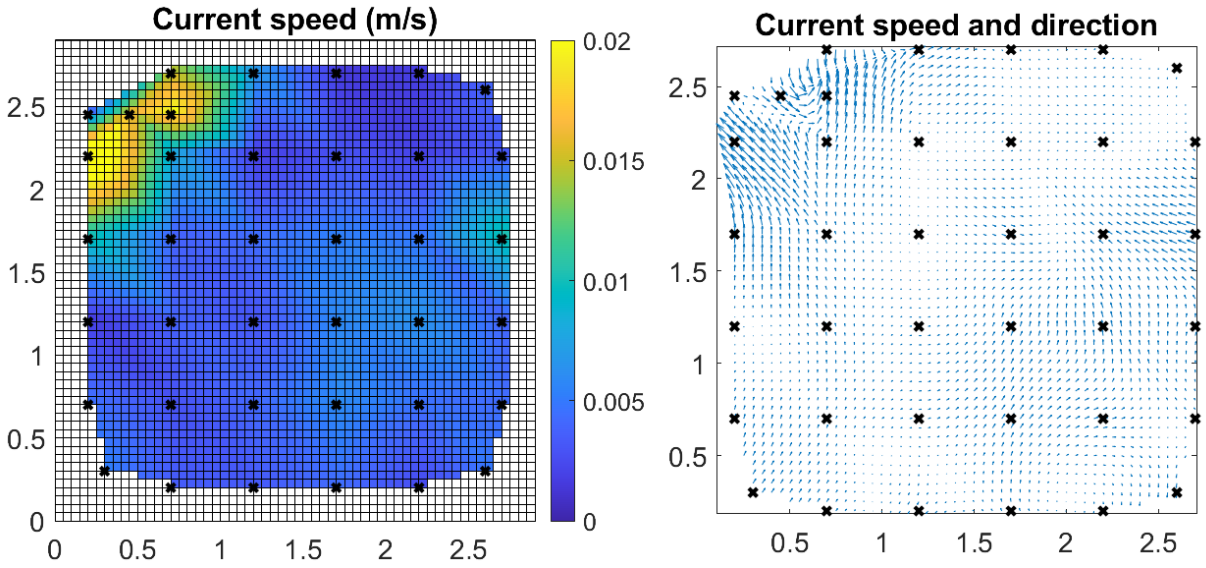

Figure 34: Interpolated current speeds and vectors in the lower plane at maximum flow.

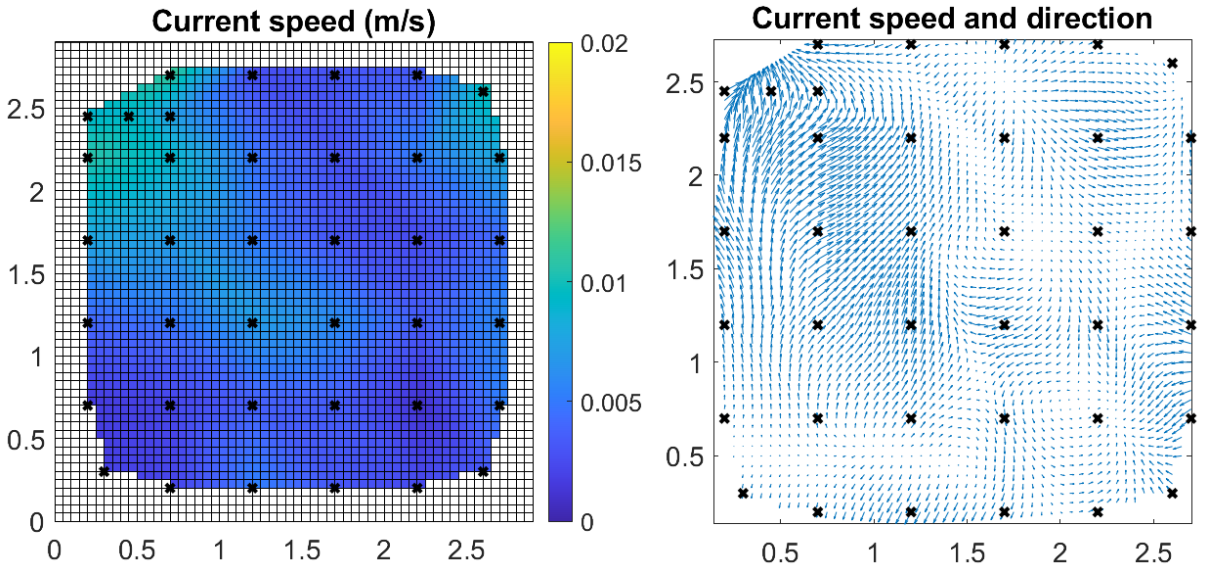

Figure 35: Interpolated current speeds and vectors in the middle plane at maximum flow.

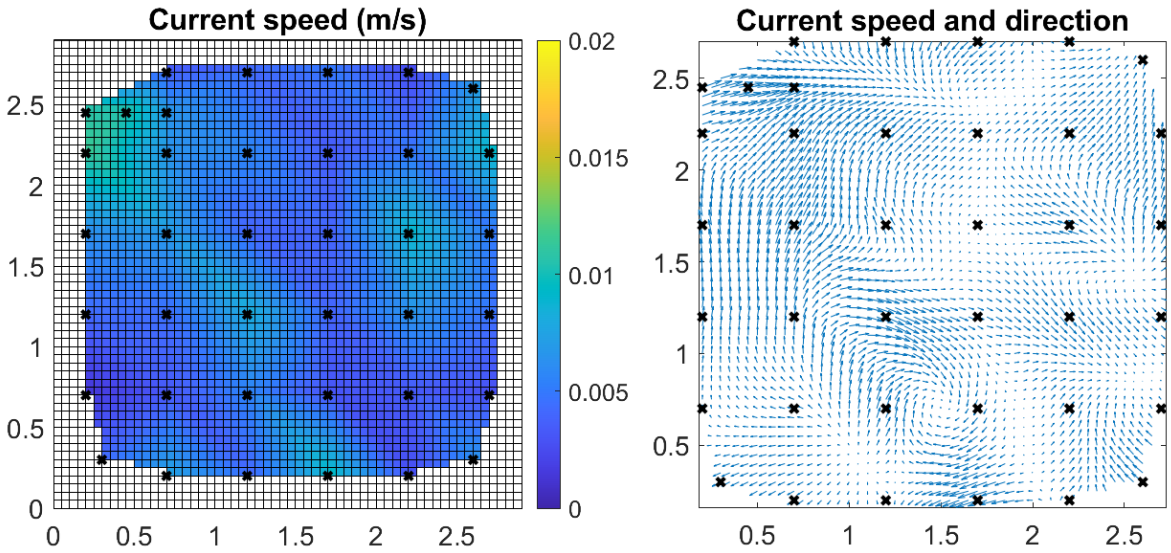

Figure 36: Interpolated current speeds and vectors in the upper plane at maximum flow.

The velocity distributions at minimum and maximum flow, summarized over all depths, are shown for the measurements in comparison to the model in Figure 37. It is obvious from the comparison that current speeds are significantly higher in the model simulations than in the measurements. The large difference is likely to be caused by the current reduction device that was installed in the tank. The device captures the momentum of the water entering the tank and makes the water enter at lower speed through the holes in the cylinder. As the system was intentionally set up to give low current speeds, the measured values are much lower than the model values.

To further test the validity of the CFD simulations, either simulations adapted to the inlet setup would have to be made, or measurements without the device would have to be made. Unfortunately, available time, funds and personnel in the AQUAEXCEL3.0 project did not allow further tests to be done.

Other studies have also measured flow velocities in fish tanks. Masaló and Oca (2014) measured current speeds in circular tanks with 0.98 m diameter and 0.23 m depth (0.69 m^3 volume) with flow rates of 0.4 and 0.72 tank volumes per hour, and found velocities ranging in the interval 0.02-0.12 m/s. Comparing to the modelled speeds in the HCMR system (original configuration), the speeds are higher than our model at minimum flow, and comparable at maximum flow. Gorle et al. (2018) measured current speeds in larger, commercial, tanks (12 m diameter, 368 m^3 volume) with a flow rate of 2.75 tank volumes per hour, and found velocities ranging in the interval 0.25-0.45 m/s, which is faster than modelled values in the HCMR system, and in between the modelled values of the INRAE original and modified systems.

Plew et al. (2015) measured current in circular tanks with 15 m diameter and 4.0-4.5 m depth (736.5 m^3 volume) with a flow rate of 0.21 tank volumes per hour, and found a mean velocity of 0.302 m/s throughout the tank. This is faster than modelled values in the HCMR tank, but of the same order as the modelled values in the INRAE tank (modified design).

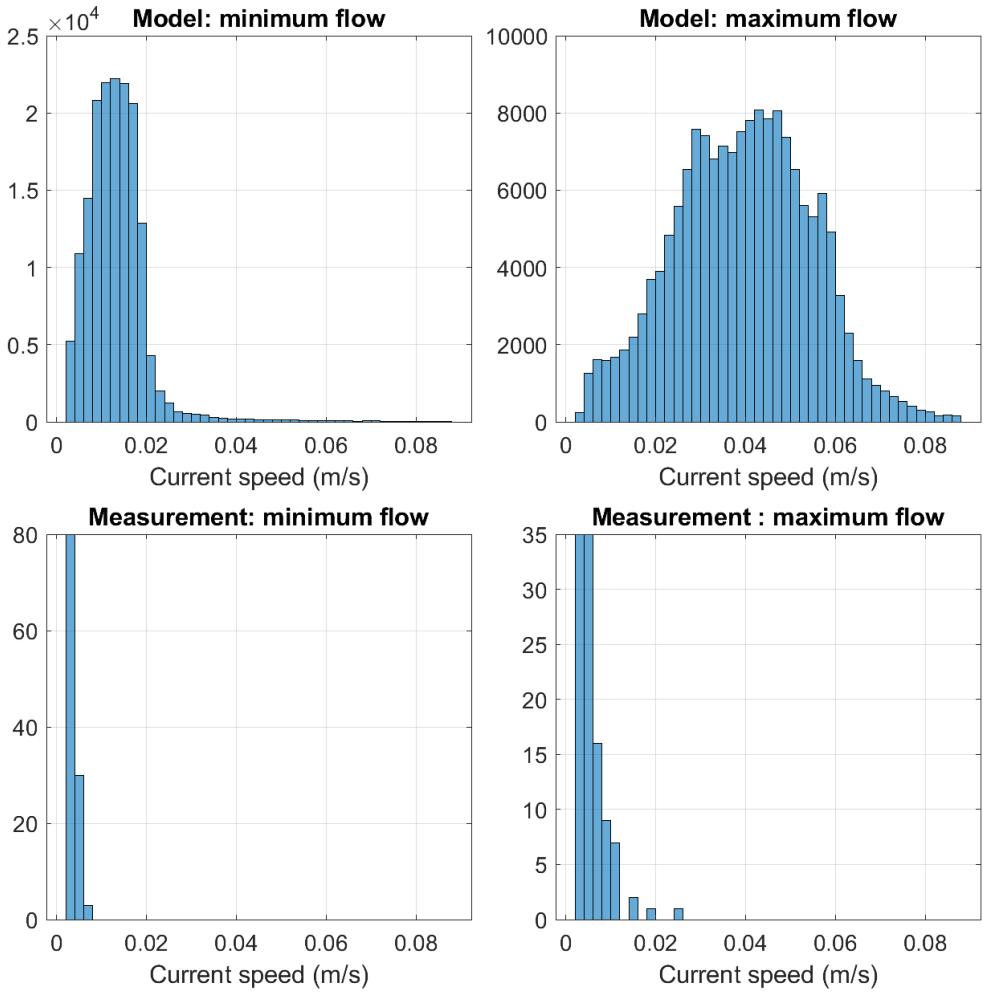

Figure 37: Statistical distributions of modelled (top) and measured (bottom) current speeds at all depths for the minimum (left) and maximum (right) flow scenarios. Values from the original HCMR 10 m^3 model configuration are shown.

4.2. Flow in sea cages

4.2.1. Average profiles

To obtain representative current speed values for Atlantic salmon cage culture in Norway, we have used numerical ocean model results calculated using the SINMOD model (Slagstad and McClimans, 2005). The regions of Middle Norway were simulated at 160 m horizontal resolution for a full year, and current statistics were found for actual aquaculture locations in the area. The simulations were done by SINTEF for the aquaculture industry, and model results are presented at the web page http://midtnorge.sinmod.com (login required for data access).

We made a selection of open locations and fjord locations, where open refers to relatively exposed locations along the coast, and fjord refers to locations inside fjords. For each of the locations, we recorded the highest and lowest monthly average current speed at every 5th m through the water column from 0-35 m. This resulted in a "high" and a "low" current profile for each location, representing high and low average values, but not extreme conditions; one can expect all of these locations to have significantly higher maximum current speeds. For each category of locations (open and fjord), we computed the mean of the high and low profiles to obtain reasonable high and low current profiles for each.

Figure 38 summarizes the high and low speeds estimated at the selected locations, as well as the mean values over the locations in each case. Both types of locations tend to have current speeds decreasing from the surface downwards, but fjord locations show a sharper transition from a shallow surface layer. This is due to stronger stratification in fjord locations compared to open locations.

4.2.2. Tidal cycles

It may be desirable for the modeler to include tidal variations in the current speed in a net cage. Tides are caused by tidal forcing from the Sun and Moon, and propagate depending on the bathymetry and coast lines in the ocean. Due to the difference in period of the forcing from the Sun (12 h) vs. the Moon (12.42 h), the weighted sum of these components leads to a near-monthly oscillation in the tidal amplitude, causing what is known as *spring* and *neap* tides. The daily oscillations in surface elevation have a period of approximately 12.2 hours. Effects with other periods also affect the signal, usually to a smaller degree. The specific tidal signal at specific locations varies greatly, and can be estimated using mathematical models. For the purposes of the Virtual Laboratory, a tidal cycle representing a typical situation is considered sufficient.

Disregarding the oscillation between *spring* and *neap* tides, a typical situation can be represented with a *sine* shaped variation in sea surface elevation. There is no need to explicitly represent the elevation, but rather the variation in current speed caused by it. Tidal current variations can be approximated by a multiplicative factor proportional to the derivative of the elevation (which is a *cosine* wave, or a *sine*

since the phase of the signal is not important here); the speed is 0 at high and low tide, and reaches a maximum as the ebb or flow rate is highest at medium elevation. When considering the absolute value of the current speed, the variation is shaped as the absolute value of a *sine* wave.

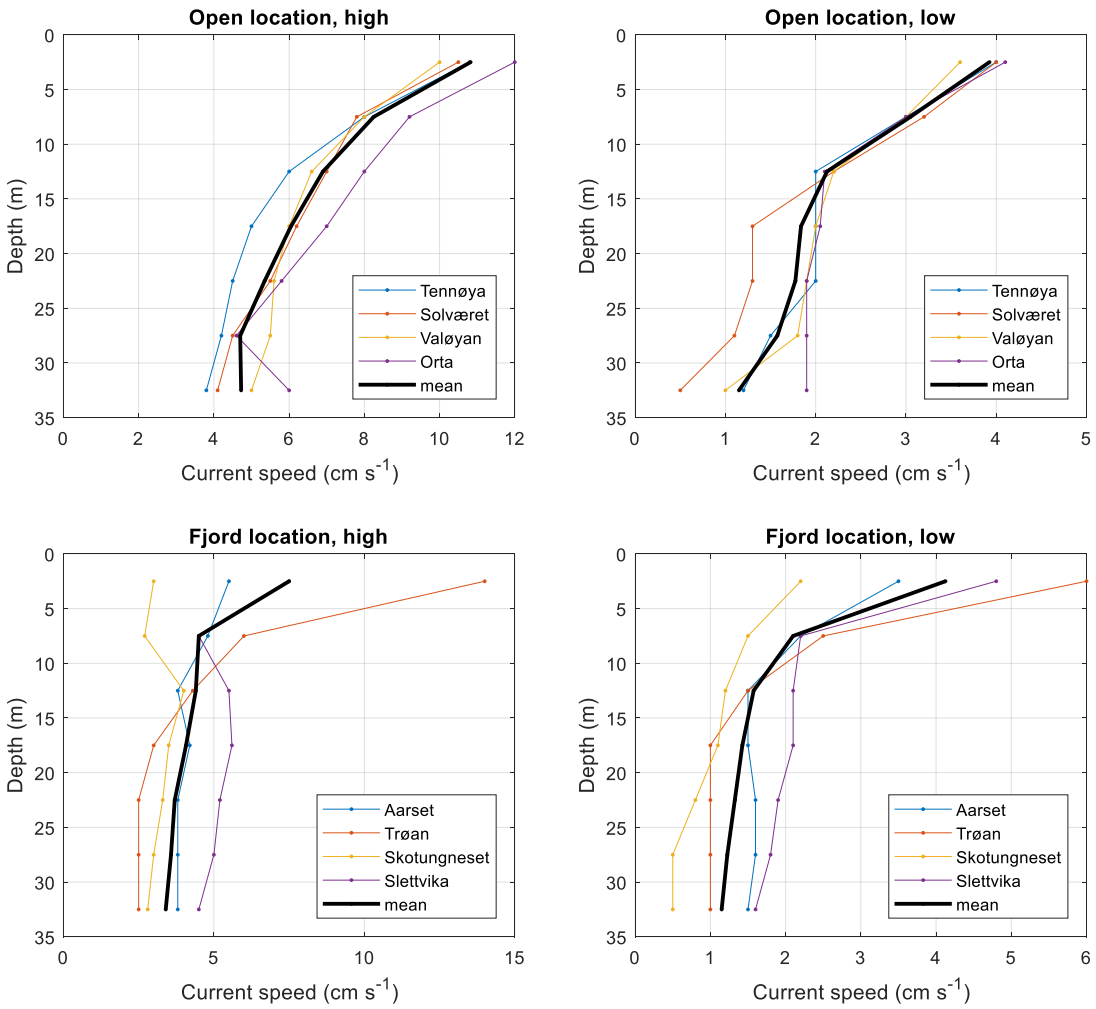

Figure 38: Representative high and low current profiles at four open locations and four fjord locations, and profiles averaged over the four locations in each case.

Since tidal variation typically accounts for only a part of the current speed at a given location, it is reasonable to add a constant value to the multiplier to ensure the current speed is not set to 0 at medium tide. Taking all this into consideration, the function for the current speed multiplier (M_{speed}) can be formulated like this:

$$M_{speed} = K_{const} + K_{tidal}|\sin(2\pi \cdot t_{hours}/12.2)| \quad (1)$$

Where K_{const} is the minimum value of the multiplier, K_{tidal} is the amplitude of the variations and t_{hours} is the time in hours.

The average value of M_{speed} is K_{const} + K_{tidal} * 2/π. Since the average current speed is set according to location type, it makes sense to design for an average multiplier value of 1. To achieve this, the parameters should be chosen according to this relationship:

$$K_{const} = 1 - K_{tidal}\frac{2}{\pi} \quad (2)$$

Figure 39 shows a time plot over 24 hours of the multiplier with K_{tidal} = 1, and K_{const} = 0.3634, chosen to get an average value of 1.

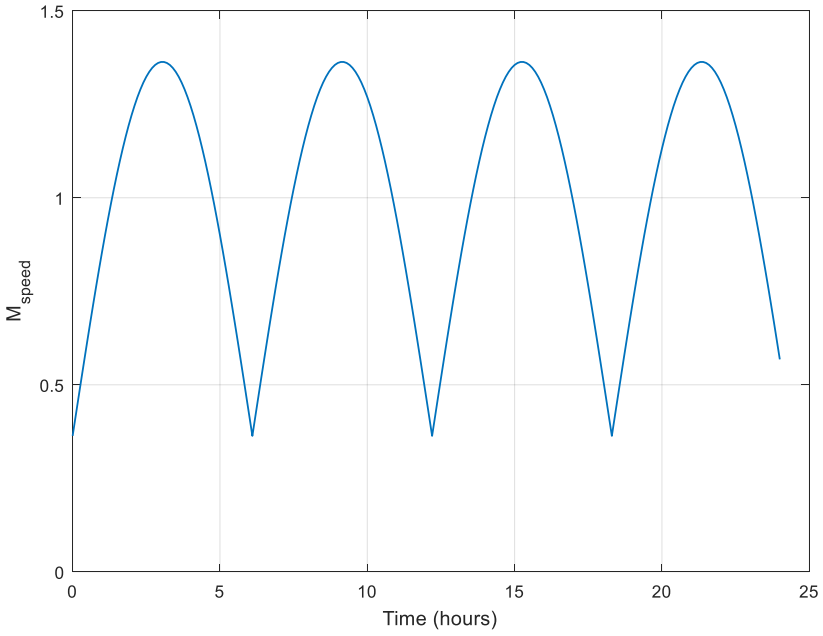

Figure 39: Tidal variations over 24 hours with Ktidal = 1 and Kconst = 0.3634. The plot shows the multiplier applied to the original speeds of the current profile to get tidally influenced speeds.

5. Conclusion

In this report, we have presented the work that has been done on the flow field model in Subtask 4.1.3 of the AQUAEXCEL3.0 project. The main results from the work in the previous AQUAEXCEL project are included for completeness, and new results are presented. Flow fields modelled using the Fluent CFD model in the HCMR and INRAE tank systems are shown along with quantitative values for turbulent kinetic energy (TKE) and estimates of the residence time of water and particles. It is shown that modification of the inlet setup has a significant impact on both TKE and residence times, and thereby can affect both the physical tank environment experienced by the fish, and the self-cleaning capacity of the tanks. A validation study was done in the HCMR system using extensive current measurements throughout the tank, but due to differences in the inlet setup, measurements indicated significantly lower current speeds than what was estimated by the CFD model. Comparison to published results from other studies indicate that the estimates of the CFD model may be in line with observed current speeds in comparable smaller and larger tank systems.

6. Appendix A

Python script for interpolation of Fluent data into onto regular grid:

```
import numpy as np
from scipy.io import netcdf_file
from scipy.interpolate import griddata
import csv

# Input and output files:
inFile = 'C:/temp/Data all cell center HCMR 10m3 Modified Design MIN flow'
outFile = 'outfile.nc'

# Data is interpolated to a 3D grid, and the dimensions of the grid are
decided here:
x_dim = 250
y_dim = 250
z_dim = 150

# Subsampling rate:
subsample = 10

nf = netcdf_file(outFile, "w")
nf.createDimension("xc", x_dim)
nf.createDimension("yc", y_dim)
nf.createDimension("zc", z_dim)
zc_var = nf.createVariable("zc", "f", ('zc',))
yc_var = nf.createVariable("yc", "f", ('yc',))
xc_var = nf.createVariable("xc", "f", ('xc',))
vel_var = nf.createVariable("velocity", "f", ('xc', 'yc', 'zc'))
u_var = nf.createVariable("u", "f", ('xc', 'yc', 'zc'))
v_var = nf.createVariable("v", "f", ('xc', 'yc', 'zc'))
w_var = nf.createVariable("w", "f", ('xc', 'yc', 'zc'))

node = []
x = []
y = []
z = []
velocity = []
xVelocity = []
yVelocity = []
zVelocity = []
axVel = []
radVel = []

first = True
with open(inFile, 'r') as csvfile:
    rd = csv.reader(csvfile, delimiter=',', quotechar='|')
    i = 0
    j = 0
```

```
    kk = 0
    for row in rd:
        i=i+1
        if first:
            first = False

        j = j+1
        if j < subsample:
            continue
        else:
            j = 0
        node.append(row[0].strip())
        xv = float(row[1]) # Fluent's x is our x
        yv = float(row[3]) # Fluent's z is our y
        zv = float(row[2]) # Fluent's y is our z
        vel = float(row[4])
        xvel = float(row[5])
        yvel = float(row[7])
        zvel = float(row[6])
        x.append(xv)
        y.append(yv)
        z.append(zv)
        velocity.append(vel)
        xVelocity.append(xvel)
        yVelocity.append(yvel)
        zVelocity.append(zvel)

print("Number of points read: ")
print(len(x))

print(str(np.min(x))+" ... "+str(np.max(x)))
print(str(np.min(y))+" ... "+str(np.max(y)))
print(str(np.min(z))+" ... "+str(np.max(z)))

x = np.asarray(x)
y = np.asarray(y)
z = np.asarray(z)
velocity = np.asarray(velocity)
xVelocity = np.asarray(xVelocity)
yVelocity = np.asarray(yVelocity)
zVelocity = np.asarray(zVelocity)

x = x - np.min(x)
y = y - np.min(y)
z = z - np.min(z)

print(str(np.min(x))+" ... "+str(np.max(x)))
print(str(np.min(y))+" ... "+str(np.max(y)))
print(str(np.min(z))+" ... "+str(np.max(z)))
x_int = np.linspace(0, np.max(x), x_dim)
y_int = np.linspace(0, np.max(y), y_dim)
z_int = np.linspace(0, np.max(z), z_dim)
```

```
grid_x, grid_y, grid_z = np.mgrid[0:x_dim, 0:y_dim, 0:z_dim]
grid_x = np.max(x)*grid_x/x_dim
grid_y = np.max(y)*grid_y/y_dim
grid_z = np.max(z)*grid_z/z_dim

xc_var[:] = x_int
yc_var[:] = y_int
zc_var[:] = z_int

print("Interpolating velocity:")
vel_int = griddata((z, y, x), velocity, (grid_z, grid_y, grid_x),
method='linear')
vel_var[:] = vel_int
print("Interpolating u:")
u_int = griddata((z, y, x), xVelocity, (grid_z, grid_y, grid_x),
method='linear')
u_var[:] = u_int
print("Interpolating v:")
v_int = griddata((z, y, x), yVelocity, (grid_z, grid_y, grid_x),
method='linear')
v_var[:] = v_int
print("Interpolating w:")
w_int = griddata((z, y, x), zVelocity, (grid_z, grid_y, grid_x),
method='linear')
w_var[:] = w_int

nf.close()
```

7. Appendix B

Header file for DLL library interface of the flow module:

```
#ifdef LIB_EXPORTS
#define LIB_API __declspec(dllexport)
#else
#define MATHLIBRARY_API __declspec(dllimport)
#endif

/*
* Open the given NetCDF file and cache its contents.
*/
extern "C" __declspec(dllexport) void openNCFile(const char* filename);

/*
* Close the opened NetCDF file.
*/
extern "C" __declspec(dllexport) void closeNCFile();

/*
* Get a 6 element matrix that gives the lower and upper bounds of the
domain in three dimensions.
*/
extern "C" __declspec(dllexport) void getDomainBounds(float* bounds);

/*
* Get the current vector at a given position.
* Return value > 0 means that the position is out of bounds.
*/
extern "C" __declspec(dllexport) int getCurrentAtPosition(float* currVec,
float x, float y, float z);
```

8. References

Alver, M.O., 2020. Final flow field model after testing period (No. D5.8), AQUAEXCEL2020.

Ansys Inc., 2021. Ansys Fluent Theory Guide.

Endresen, P.C., Føre, M., Fredheim, A., Kristiansen, D., Enerhaug, B., 2013. Numerical modeling of wake effect on aquaculture nets, in: International Conference on Offshore Mechanics and Arctic Engineering. American Society of Mechanical Engineers, p. V003T05A027.

Gorle, J.M.R., Terjesen, B.F., Mota, V.C., Summerfelt, S., 2018. Water velocity in commercial RAS culture tanks for Atlantic salmon smolt production. Aquac. Eng. 81, 89–100.

Klebert, P., Lader, P., Gansel, L., Oppedal, F., 2013. Hydrodynamic interactions on net panel and aquaculture fish cages: A review. Ocean Eng. 58, 260–274. https://doi.org/10.1016/j.oceaneng.2012.11.006

Løland, G., 1993. Current forces on, and water flow through and around, floating fish farms. Aquac. Int. 1, 72–89.

Masaló, I., Oca, J., 2014. Hydrodynamics in a multivortex aquaculture tank: Effect of baffles and water inlet characteristics. Aquac. Eng. 58, 69–76. https://doi.org/10.1016/j.aquaeng.2013.11.001

Papáček, Š., Petera, K., Císař, P., Stejskal, V., Saberioon, M., 2020. Experimental & Computational Fluid Dynamics Study of the Suitability of Different Solid Feed Pellets for Aquaculture Systems. Appl. Sci. 10. https://doi.org/10.3390/app10196954

Plew, D.R., Klebert, P., Rosten, T.W., Aspaas, S., Birkevold, J., 2015. Changes to flow and turbulence caused by different concentrations of fish in a circular tank. J. Hydraul. Res. 53, 364–383. https://doi.org/10.1080/00221686.2015.1029016

Reite, K.-J., Føre, M., Aarsæther, K.G., Jensen, J., Rundtop, P., Kyllingstad, L.T., Endresen, P.C., Kristiansen, D., Johansen, V., Fredheim, A., 2014. Fhsim—time domain simulation of marine systems, in: International Conference on Offshore Mechanics and Arctic Engineering. American Society of Mechanical Engineers, p. V08AT06A014.

Sayma, A., 2009. Computational fluid dynamics. Bookboon.

Shchepetkin, A.F., McWilliams, J.C., 2005. The regional oceanic modeling system (ROMS): a split-explicit, free-surface, topography-following-coordinate oceanic model. Ocean Model. 9, 347–404.

Slagstad, D., McClimans, T.A., 2005. Modeling the ecosystem dynamics of the Barents Sea including the marginal ice zone: I. Physical and chemical oceanography. J. Mar. Syst. 58, 1–18.

Timmons, M.B., Summerfelt, S.T., Vinci, B.J., 1998. Review of circular tank technology and management. Aquac. Eng. 18, 51–69. https://doi.org/10.1016/S0144-8609(98)00023-5

Document Information

EU Project	No 871108	Acronym	AQUAEXCEL3.0
Full Title	AQUAculture infrastructures for EXCELlence in European fish research 3.0		
Project website	www.aquaexcel.eu		

Deliverable	N°	D4.5	Title	Modelled flow fields, turbulence and residence time in experimental units
Work Package	N°	4	Title	JRA1 - Technological tools for improved experimental procedures
Work Package Leader	Finn Olav Bjørnson			
Work Participants	NTNU, JU, NOFIMA, SINTEF			

Lead Beneficiary	NTNU, Partner 10
Authors	Morten Omholt Alver, NTNU, morten.alver@ntnu.no; Khurram Shazad, NOFIMA Orestis Stavrakidis-Zachou, HCMR; Andrei Tsarau, SINTEF
Reviewers	Finn Olav Bjørnson, SINTEF Ocean, finn.o.bjornson@sintef.no Wout Abbink, WUR, wout.abbink@wur.nl

Due date of deliverable	30.09.2024
Submission date	30.09.2024
Dissemination level	PU
Type of deliverable	R-Other

Version log			
Issue Date	Revision N°	Author	Change
31.08.2024	1	Morten Omholt Alver	First version for internal review
15.09.2024	2	Morten Omholt Alver	Updates based on internal review
01.10.2024	3	Morten Omholt Alver	Updates based on coordinator review